White Rose Research Online

eprints@whiterose.ac.uk
https://eprints.whiterose.ac.uk
Universities of Leeds, Sheffield and York

Deposited via The University of Leeds.

White Rose Research Online URL for this paper:
https://eprints.whiterose.ac.uk/id/eprint/99465/

Version: Accepted Version

Article:
Marin, L, Karageorghis, A, Lesnic, D et al. (2017) The method of fundamental solutions for problems in static thermo-elasticity with incomplete boundary data. Inverse Problems in Science and Engineering, 25 (5). pp. 652-673. ISSN: 1741-5977

https://doi.org/10.1080/17415977.2016.1191072

© 2016 Informa UK Limited, trading as Taylor & Francis Group. This is an Accepted Manuscript of an article published by Taylor & Francis in Inverse Problems in Science and Engineering on 7 June 2016, available online: http://www.tandfonline.com/10.1080/17415977.2016.1191072. Uploaded in accordance with the publisher's self-archiving policy.

Reuse
Items deposited in White Rose Research Online are protected by copyright, with all rights reserved unless indicated otherwise. They may be downloaded and/or printed for private study, or other acts as permitted by national copyright laws. The publisher or other rights holders may allow further reproduction and re-use of the full text version. This is indicated by the licence information on the White Rose Research Online record for the item.

Takedown
If you consider content in White Rose Research Online to be in breach of UK law, please notify us by emailing eprints@whiterose.ac.uk including the URL of the record and the reason for the withdrawal request.

UNIVERSITY OF LEEDS
University of Sheffield
UNIVERSITY of York

THE METHOD OF FUNDAMENTAL SOLUTIONS FOR PROBLEMS IN STATIC THERMO-ELASTICITY WITH INCOMPLETE BOUNDARY DATA

L. MARIN, A. KARAGEORGHIS, D. LESNIC, AND B. T. JOHANSSON

Abstract. An inverse problem in static thermo-elasticity is investigated. The aim is to reconstruct the unspecified boundary data, as well as the temperature and displacement inside a body from over-specified boundary data measured on an accessible portion of its boundary. The problem is linear but ill-posed. The uniqueness of the solution is established but the continuous dependence on the input data is violated. In order to reconstruct a stable and accurate solution, the method of fundamental solutions is combined with Tikhonov regularization where the regularization parameter is selected based on the L-curve criterion. Numerical results are presented in both two and three dimensions showing the feasibility and ease of implementation of the proposed technique.

1. Introduction

In many practical applications that involve the determination of the temperature and displacement in structures of aircraft and propulsion systems, gas and steam turbines, or in chemical and nuclear reactors, measurements are possible only on an accessible part of the boundary. This can be caused by the physical environment or harsh conditions encountered which prevents the boundary conditions from being specified, prescribed or measured over the whole of the boundary of the body under consideration. The physical situation described above gives rise to inverse boundary value problems in which the thermo-elastic fields in the body and on the inaccessible boundary have to be determined from over-prescribed displacement and traction measurements taken on a portion of the accessible boundary.

Some previous research concerned inverse steady-state, quasi-static and dynamic thermo-elastic analyses. For example, early studies by Noda [26] and Noda et al. [27] investigated inverse transient thermo-elastic problems in an infinitely long cylinder and in a transversely-isotropic body, respectively. Later on, Lee and Yang [20] and Yang et al. [31] investigated inverse problems predicting the heat flux and thermal stresses from strain measurements in an infinitely long annular cylinder, whilst Khajehpour and Hematiyan [18] presented a domain decomposition inverse analysis for solving a thermo-elastic problem under a thermal shock.

Quasi-static inverse estimation of missing boundary conditions in thermo-elastic functionally graded and nonlinear temperature materials have been considered by Tanaka et al. [30] using the dual reciprocity boundary element method (DRBEM).

As far as the steady-state inverse thermo-elasticity analysis is concerned, numerical research in two and three dimensions was initiated in [8, 9], with much earlier theoretical uniqueness results being established in [19] (where the quasi-static and dynamic cases were also addressed).

Recently, the authors have solved numerically the inverse boundary value problem in static thermo-elasticity proposed in [19] using the method of fundamental solutions (MFS) [16, 23, 24]. In the present paper, we consider a similar type but different inverse formulation of the previously investigated problem for which we have also been able to prove the uniqueness of solution in Section 2. Furthermore, the numerical solution of the problem based

Date: April 24, 2016.
2000 *Mathematics Subject Classification.* Primary 33A65, 65N35; Secondary 65N22, 65F05, 35J05.
Key words and phrases. thermo-elasticity; method of fundamental solutions; inverse problem.

on the MFS combined with the Tikhonov regularization method (TRM) is attempted in Section 3. This yields accurate and stable results in both two and three dimensions as illustrated in Section 4. Finally, conclusions and ideas for future work are presented in Section 5.

2. Mathematical formulation

We consider a homogeneous, linear-elastic and isotropic body occupying a simply-connected domain $\Omega \subset \mathbb{R}^{\mathrm{n}}, \mathrm{n} = 2, 3$, bounded by a smooth boundary $\partial\Omega$. For simplicity, we assume that internal heat sources and other body forces are absent. Then, in the static regime, the equations of thermo-elasticity read as, see [29],

$$\mathcal{A}\boldsymbol{u} := G\left[\nabla\cdot\left(\nabla\boldsymbol{u} + (\nabla\boldsymbol{u})^{\mathrm{T}}\right) + \frac{2\,\overline{\nu}}{1-2\,\overline{\nu}}\,\nabla\left(\nabla\cdot\boldsymbol{u}\right)\right] = \gamma\,\nabla T \qquad \text{in} \qquad \Omega. \tag{2.1}$$

$$\kappa\,\Delta T = 0 \qquad \text{in} \qquad \Omega, \tag{2.2}$$

where $\kappa > 0$ is the thermal conductivity and

$$\gamma = \frac{2\,(1+\overline{\nu})\;\overline{\alpha}_T\,G}{1-2\,\overline{\nu}},$$

$$\overline{\nu} = \begin{cases} \nu & \text{plane strain} \quad (\mathrm{n}=2) \text{ or } \mathrm{n}=3, \\ \dfrac{\nu}{1+\nu} & \text{plane stress} \qquad (\mathrm{n}=2), \end{cases}$$

$$\overline{\alpha}_T = \begin{cases} \alpha_T & \text{plane strain} \quad (\mathrm{n}=2) \text{ or } \mathrm{n}=3, \\ \dfrac{\alpha_T\,(1+\nu)}{1+2\,\nu} & \text{plane stress} \qquad (\mathrm{n}=2), \end{cases}$$

T is the temperature, $\boldsymbol{u}$ is the displacement, G is the shear modulus, α_T is the coefficient of thermal expansion and $\nu \in (0, 1/2)$ is the Poisson ratio. In (2.2), the thermal conductivity κ has been assumed to be constant, i.e. equal to its value at average temperature. More general space or temperature variations of κ could also be considered, see the numerical implementations in [30] and [18], but for our theoretical study of uniqueness of a solution and for the MFS implementation these more complex cases are deferred to a future work.

The heat flux and the traction on the boundary are defined, respectively, as

$$q := -\kappa\,\nabla T\cdot\boldsymbol{n} \qquad \text{on} \qquad \partial\Omega, \tag{2.3}$$

$$\boldsymbol{t} := \boldsymbol{\sigma}(\boldsymbol{u})\,\boldsymbol{n} = \widehat{\boldsymbol{\sigma}}(\boldsymbol{u})\,\boldsymbol{n} - \gamma\,T\,\boldsymbol{n}, \qquad \text{on} \qquad \partial\Omega, \tag{2.4}$$

where $\boldsymbol{\sigma}(\boldsymbol{u})$ is the stress tensor, $\boldsymbol{n}$ is the outward unit normal to the boundary and $\widehat{\boldsymbol{\sigma}}(\boldsymbol{u})$ is the so-called pseudo-stress tensor, [28], given by

$$\widehat{\boldsymbol{\sigma}}(\boldsymbol{u}) = 2\,G\left[\boldsymbol{\varepsilon} + \frac{\overline{\nu}}{1-2\,\overline{\nu}}\mathrm{tr}(\boldsymbol{\varepsilon})\boldsymbol{I}\right], \tag{2.5}$$

where $\boldsymbol{I}$ is the identity tensor and $\mathrm{tr}(\boldsymbol{\varepsilon})$ denotes the trace of the strain tensor which is defined by

$$\boldsymbol{\varepsilon}(\boldsymbol{u}) = \frac{1}{2}\left(\nabla\boldsymbol{u} + (\nabla\boldsymbol{u})^{\mathrm{T}}\right). \tag{2.6}$$

We assume that the displacement is specified over the whole boundary $\partial\Omega$, i.e.

$$\boldsymbol{u} = \boldsymbol{f} \qquad \text{on} \qquad \partial\Omega, \tag{2.7}$$

where $\boldsymbol{f}$ is a specified vector function.

If T is prescribed on the whole boundary $\partial\Omega$ then this gives rise to the direct problem of thermo-elasticity which is well-posed, see e.g. [12]. However, in our inverse problem, only the part Γ_1 (assumed non-empty open) of

$\partial\Omega$ is accessible to measurement and on it we assume that both the heat flux and the traction are known by measurements, namely, we have the supplementary conditions

$$-\kappa \frac{\partial T}{\partial n} = \widetilde{q} \qquad \text{on} \qquad \Gamma_1, \tag{2.8}$$

$$\boldsymbol{t} = \widetilde{\boldsymbol{t}} \qquad \text{on} \qquad \Gamma_1, \tag{2.9}$$

where $\widetilde{q}$ and $\widetilde{\boldsymbol{t}}$ are specified functions on Γ_1. We note that the related inverse problem given by equations (2.1), (2.2) subject to the boundary conditions

$$\boldsymbol{t} = \widetilde{\boldsymbol{t}} \qquad \text{on} \qquad \partial\Omega, \tag{2.10}$$

$$\boldsymbol{u} = \boldsymbol{f} \qquad \text{on} \qquad \Gamma_1, \tag{2.11}$$

$$T = \widetilde{T} \qquad \text{on} \qquad \Gamma_1, \tag{2.12}$$

has been investigated theoretically in [19]. For completeness, we mention the Cauchy problem given by equations (2.1), (2.2), (2.7), (2.8) and (2.12) which has been investigated in [15].

A regularized MFS has been proposed by the authors for solving the problem given by equations (2.1), (2.2), (2.7), (2.8) and (2.12) in [22] and the problem given by equations (2.1), (2.2), (2.10)–(2.12) in [16] and it is the purpose of the present study to develop the same method for solving the new inverse problem given by equations (2.1), (2.2), (2.7)-(2.9). One can remark that both these inverse problems can also be solved iteratively by minimizing the least squares gap $\frac{1}{2}\|\boldsymbol{u}-\boldsymbol{f}\|_{(L^2(\Gamma_1))^n}$ with respect to $T|_{\Gamma_2}$, where $\Gamma_2 := \partial\Omega\backslash\Gamma_1$. However, for the inverse problem (2.1), (2.2), (2.10)–(2.12), the corresponding direct problem is of Neumann traction type (2.10) and the additional rigid body motion has to be factorized in order to obtain a unique solution, whilst for the inverse problem (2.1), (2.2), (2.7)-(2.9) which is investigated in this study, the corresponding direct problem is of mixed type (with traction specification (2.9) on Γ_1 and displacement $\boldsymbol{u} = \boldsymbol{f}$ on Γ_2) and hence it has at most one solution. Another new contribution in this paper is that we establish the uniqueness of solution of the inverse problem (2.1), (2.2), (2.7)-(2.9), as described next.

2.1. **Uniqueness of solution.** First, we remark that in the one-dimensional case $\Omega = (0,1)$, the problem given by equations (2.1), (2.2), (2.7)-(2.9) with $\Gamma_1 = \{0\}$ becomes

$$\begin{cases} \dfrac{2\,G\,(1-\overline{\nu})}{1-2\,\overline{\nu}}\dfrac{d^2u}{dx^2} = \gamma\,\dfrac{dT}{dx}, & x \in (0,1), \\ \dfrac{d^2T}{dx^2} = 0, & x \in (0,1), \\ u(0) = u(1) = 0, \\ T'(0) = 0, \\ \dfrac{2\,G\,(1-\overline{\nu})}{1-2\,\overline{\nu}}u'(0) - \gamma\,T(0) = 0. \end{cases} \tag{2.13}$$

If the last condition in (2.13) is dropped, we obtain the nontrivial solution $(u(x), T(x)) = (0, \xi)$ with arbitrary $\xi \in \mathbb{R}$, whilst if the condition before last in (2.13) is dropped we obtain the nontrivial solution

$$(u(x), T(x)) = \left(\frac{(1-2\overline{\nu})\gamma\xi}{4G(1-\overline{\nu})}\,(x^2-x),\ \xi\left(x-\frac{1}{2}\right)\right).$$

This shows that the supplementary conditions (2.8) and (2.9) are essential for the uniqueness of solution of the inverse problem.

Integrating the full system of equations (2.13) we obtain

$$\begin{cases} \gamma\, T(x) = \dfrac{2\,G\,(1-\overline{\nu})}{1-2\,\overline{\nu}}\dfrac{du}{dx}(x), & x \in (0,1), \\ \\ T(x) = \text{constant}, & x \in (0,1), \end{cases}$$

which upon imposing $u(0) = u(1) = 0$ readily yield $T = 0 = u$ in Ω.

In higher dimensions we prove the following uniqueness theorem.

Theorem 1. *The inverse problem given by equations* (2.1), (2.2), (2.7)-(2.9) *has at most one solution.*

Proof. Assuming that there are two solutions and taking their differences, proving uniqueness becomes equivalent to showing that the only solution of equations (2.1) and (2.2) subject to the homogeneous boundary conditions (2.7)-(2.9), i.e.

$$\boldsymbol{u} = \boldsymbol{0} \qquad \text{on} \qquad \partial\Omega, \tag{2.14}$$

$$-\,\kappa\,\frac{\partial T}{\partial n} = 0 \qquad \text{on} \qquad \Gamma_1, \tag{2.15}$$

$$\boldsymbol{t} = \boldsymbol{0} \qquad \text{on} \qquad \Gamma_1, \tag{2.16}$$

is the trivial solution $\boldsymbol{u} = \boldsymbol{0}$ and $T = 0$ in Ω.

We follow similar ideas to those in the proof of Theorem 1 in [19] for the uniqueness of solution of the inverse problem given by equations (2.1), (2.2), (2.10)–(2.12). Assume sufficient smoothness to work with classical functions.

First, we construct $\boldsymbol{w}$ as a solution of

$$G\,\Delta\boldsymbol{w}(\boldsymbol{x}) = \boldsymbol{m}\,\delta(\boldsymbol{x}-\boldsymbol{y}), \qquad \boldsymbol{x} \in \mathbb{R}^{\mathrm{n}}, \tag{2.17}$$

where $\boldsymbol{m}$ is a given and fixed (constant) vector in $\mathbb{R}^{\mathrm{n}}, \mathrm{n} = 2, 3$, δ is the Dirac delta function and $\boldsymbol{y}$ is an arbitrary fixed point in $\mathbb{R}^{\mathrm{n}}$.

Recall Betti's formula in elasticity

$$\int_\Omega \left(\boldsymbol{v}\cdot\mathcal{A}\boldsymbol{u} - \boldsymbol{u}\cdot\mathcal{A}\boldsymbol{v}\right)\,d\Omega = \int_{\partial\Omega}\left[\boldsymbol{v}\cdot\widehat{\boldsymbol{\sigma}}(\boldsymbol{u})\boldsymbol{n} - \boldsymbol{u}\cdot\widehat{\boldsymbol{\sigma}}(\boldsymbol{v})\boldsymbol{n}\right]\,dS, \tag{2.18}$$

where the operator $\mathcal{A}$ is defined in (2.1). We remark that

$$\mathcal{A}\boldsymbol{w} = G\,\Delta\boldsymbol{w} + \frac{G}{1-2\,\overline{\nu}}\,\nabla\left(\nabla\cdot\boldsymbol{w}\right) = \boldsymbol{m}\,\delta(\boldsymbol{x}-\boldsymbol{y}) + \frac{G}{1-2\,\overline{\nu}}\,\nabla\left(\nabla\cdot\boldsymbol{w}\right),$$

and also that for $\boldsymbol{v} := \nabla\times\boldsymbol{w}$ we have

$$\mathcal{A}\,\boldsymbol{v} = \mathcal{A}\,\nabla\times\boldsymbol{w} = \nabla\times\left(\boldsymbol{m}\,\delta(\boldsymbol{x}-\boldsymbol{y})\right) + \frac{G}{1-2\,\overline{\nu}}\nabla\times\left(\nabla\left(\nabla\cdot\boldsymbol{w}\right)\right) = \nabla\times\left(\boldsymbol{m}\,\delta(\boldsymbol{x}-\boldsymbol{y})\right),$$

since the curl of a gradient is equal to zero. Then, applying (2.18) for $\boldsymbol{u}$ satisfying equations (2.1) and (2.2) and $\boldsymbol{v} = \nabla\times\boldsymbol{w}$ we obtain

$$\begin{aligned}\int_\Omega\left[\gamma\,\nabla T\cdot\boldsymbol{v} - \left(\nabla\times\left(\boldsymbol{m}\,\delta(\boldsymbol{x}-\boldsymbol{y})\right)\right)\cdot\boldsymbol{u}\right]\,d\Omega &= \int_{\partial\Omega}\left[\boldsymbol{v}\cdot\widehat{\boldsymbol{\sigma}}(\boldsymbol{u})\,\boldsymbol{n} - \boldsymbol{u}\cdot\widehat{\boldsymbol{\sigma}}(\boldsymbol{v})\,\boldsymbol{n}\right]\,dS \\ &= \int_{\Gamma_1}\gamma\,T\,\boldsymbol{n}\cdot\boldsymbol{v}\,d\Gamma_1 + \int_{\Gamma_2}\boldsymbol{v}\cdot\widehat{\boldsymbol{\sigma}}(\boldsymbol{u})\boldsymbol{n}\,d\Gamma_2,\end{aligned} \tag{2.19}$$

where use has been made of the homogeneous Dirichlet boundary condition (2.14) on $\partial\Omega$. Now, using Gauss' divergence formula for the vectorial function $T\boldsymbol{v}$, Stokes' theorem and that the divergence of the curl is zero, we obtain that the left-hand side of (2.19) is equal to

$$\int_{\Gamma_1}\gamma\,T\,\boldsymbol{n}\cdot\boldsymbol{v}\,d\Gamma_1 + \int_{\Gamma_2}\gamma\,T\,\boldsymbol{n}\cdot\boldsymbol{v}\,d\Gamma_2 + \int_\Omega\delta(\boldsymbol{x}-\boldsymbol{y})\,\boldsymbol{m}\cdot\left(\nabla\times\boldsymbol{u}\right)\,d\Omega - \int_{\partial\Omega}\delta(\boldsymbol{x}-\boldsymbol{y})\,\boldsymbol{m}\cdot\boldsymbol{u}\,dS.$$

Taking $\boldsymbol{y} \notin \partial\Omega$, the last boundary integral vanishes and equation (2.19) simplifies to

$$\int_{\Gamma_2} (\widehat{\boldsymbol{\sigma}}(\boldsymbol{u})\,\boldsymbol{n} - \gamma\, T\,\boldsymbol{n}) \cdot \boldsymbol{v}(\boldsymbol{x};\boldsymbol{y})\, d\Gamma_2 = \begin{cases} \boldsymbol{m} \cdot \nabla \times \boldsymbol{u}(\boldsymbol{y}) & \text{if} \quad \boldsymbol{y} \in \Omega, \\ \\ 0 & \text{if} \quad \boldsymbol{y} \in \mathbb{R}^{\mathrm{n}} \backslash \overline{\Omega}. \end{cases}$$

From this identity, it follows that the left-hand side is a harmonic function in $\boldsymbol{y}$, which is zero in $\mathbb{R}^{\mathrm{n}}\backslash\overline{\Omega}$ (which is connected because Ω is simply connected) and is smooth across Γ_1. From standard unique continuation results for harmonic functions it follows that the above expression is also identically zero in $\overline{\Omega}$. Therefore,

$$\boldsymbol{m} \cdot (\nabla \times \boldsymbol{u}(\boldsymbol{y})) = 0 \quad \text{in} \quad \Omega,$$

and, since $\boldsymbol{m}$ is arbitrary,

$$\nabla \times \boldsymbol{u}(\boldsymbol{y}) = \boldsymbol{0} \quad \text{in} \quad \Omega.$$

This means that $\boldsymbol{u}$ is an irrotational field and since Ω is simply connected it follows that there exists a potential function φ such that $\boldsymbol{u} = \nabla\varphi$, see e.g. [7, Corollary 3, p.217]. Using this in equation (2.1) we get that

$$\frac{2\,G\,(1-\overline{\nu})}{1-2\,\overline{\nu}}\,\nabla\,(\Delta\varphi) = \gamma\,\nabla T \qquad \text{in} \qquad \Omega, \tag{2.20}$$

and integrating, we obtain

$$\frac{2\,G\,(1-\overline{\nu})}{1-2\,\overline{\nu}}\,\Delta\varphi = \gamma\,T + c \qquad \text{in} \qquad \Omega. \tag{2.21}$$

where c is some constant.

Since $\boldsymbol{u} = \boldsymbol{0}$ on $\partial\Omega$, see (2.14), and $\boldsymbol{u} = \nabla\varphi$ we can conclude that $\varphi = c_0$ =constant on $\partial\Omega$. Without loss of generality we can assume that

$$\varphi = 0 \qquad \text{in} \qquad \partial\Omega. \tag{2.22}$$

Taking the Laplace operator in equation (2.21) and using equation (2.2) we obtain that the function φ is biharmonic, i.e.

$$\Delta^2\varphi = 0 \quad \text{in} \quad \Omega, \tag{2.23}$$

satisfying

$$\varphi = 0, \quad \frac{\partial\varphi}{\partial n} = 0 \quad \text{on} \quad \partial\Omega. \tag{2.24}$$

Problem (2.23) and (2.24) is a direct Dirichlet problem for the biharmonic equation the solution of which is

$$\varphi = 0 \quad \text{in} \quad \overline{\Omega}. \tag{2.25}$$

Since $\boldsymbol{u} = \nabla\varphi$, we have shown that

$$\boldsymbol{u} = \boldsymbol{0} \quad \text{in} \quad \overline{\Omega}.$$

Then, from (2.1) and (2.2), we obtain

$$\nabla T = \boldsymbol{0} \quad \text{and} \quad \Delta T = 0 \quad \text{in} \quad \Omega$$

which yields that T =constant= C.
Further, from (2.15) we have

$$\boldsymbol{0} = \widehat{\boldsymbol{\sigma}}(\boldsymbol{u})\,\boldsymbol{n} = \gamma\, T\boldsymbol{n} \quad \text{on} \quad \partial\Omega,$$

which immediately yields that $C = 0$. Thus $T = 0$, which concludes the uniqueness proof. □

Even though this theorem ensures the uniqueness of solution, the inverse problem (2.1), (2.2), (2.7)-(2.9) is still ill-posed since small errors in the input data cause large errors in the output solution. This instability can be seen as follows. Assuming a known boundary temperature on Γ_2, say $T = T_0$ on Γ_2, then one can directly obtain the temperature T (as a function of T_0) in $\overline{\Omega}$, and its gradient ∇T in Ω, by solving a mixed well-posed problem for the Laplace equation (2.2) with the Neumann boundary condition (2.8) on Γ_1 and the Dirichlet boundary condition $T = T_0$ on Γ_2. What then remains is a data completion problem for the displacement $\boldsymbol{u}$ in the elliptic equation $\mathcal{A}\boldsymbol{u} = \gamma\,\nabla T$, with known right-hand side, where from displacement and pseudo-traction $(\widehat{\boldsymbol{t}} = \widehat{\boldsymbol{\sigma}}(\boldsymbol{u})\,\boldsymbol{n} = \widetilde{\boldsymbol{t}} + \gamma\, T|_{\Gamma_1}\boldsymbol{n})$

values on Γ_1, one has to find the correct boundary function T_0 on Γ_2 (since the pseudo-traction on Γ_1 will depend on T_0) to match the given displacement on Γ_2. This type of data completion is a classical Cauchy problem for an elliptic equation, which is well-known to be ill-posed with respect to the noise in the data, see further [1]. In a more technical language, one can build on this to reformulate problem (2.1), (2.2), (2.7)-(2.9) as an operator equation on the boundary with the linear operator having an unbounded inverse. The details for this, however, are outside the scope of this work. Likewise, the interesting challenge of finding classes of functions satisfying uniform bounds and for which stability can be restored in (2.1), (2.2), (2.7)-(2.9) will not be investigated in this study.

In the next section we describe the application of the MFS for the solution of the inverse and ill-posed linear problem (2.1), (2.2), (2.7)-(2.9).

An alternative to the MFS is the boundary element method (BEM), see [13], which eliminates the need for selecting exterior sources but requires the evaluation of boundary integrals. Moreover, if the mechanical and/or thermal properties are space- or temperature-dependent, then one can employ the finite element method (FEM), see [10], or the DRBEM, see [30].

3. The method of fundamental solutions (MFS)

In the application of the MFS to the thermo-elasticity system [17, 21], first, the harmonic temperature is sought as a linear combination of non-singular fundamental solutions

$$T_N(\boldsymbol{x}) = \sum_{\ell=1}^{N} c_\ell \, F(\boldsymbol{x}, \boldsymbol{\xi}_\ell), \qquad \boldsymbol{x} \in \overline{\Omega}, \tag{3.1}$$

where $(c_\ell)_{\ell=\overline{1,N}}$ are unknown coefficients, the sources $(\boldsymbol{\xi}_\ell)_{\ell=\overline{1,N}} \notin \overline{\Omega}$ and

$$F(\boldsymbol{x}, \boldsymbol{\xi}_\ell) = \begin{cases} -\dfrac{1}{2\pi\,\kappa} \, \log|\boldsymbol{x} - \boldsymbol{\xi}| & \text{if} \quad \text{n} = 2, \\ \dfrac{1}{4\pi\,\kappa\,|\boldsymbol{x} - \boldsymbol{\xi}|} & \text{if} \quad \text{n} = 3, \end{cases} \tag{3.2}$$

is the fundamental solution of Laplace's equation.

Using equations (2.3), (3.1) and (3.2), we can also derive an approximation for the heat flux

$$q_N(\boldsymbol{x}) = -\kappa \, \frac{\partial T_N}{\partial n}(\boldsymbol{x}) = \begin{cases} \dfrac{1}{2\,\pi} \displaystyle\sum_{\ell=1}^{N} c_\ell \, \frac{(\boldsymbol{x} - \boldsymbol{\xi}_\ell) \cdot \boldsymbol{n}(\boldsymbol{x})}{|\boldsymbol{x} - \boldsymbol{\xi}|^2} & \text{if} \quad \text{n} = 2 \\ \\ \dfrac{1}{4\pi} \displaystyle\sum_{\ell=1}^{N} c_\ell \, \frac{(\boldsymbol{x} - \boldsymbol{\xi}_\ell) \cdot \boldsymbol{n}(\boldsymbol{x})}{|\boldsymbol{x} - \boldsymbol{\xi}|^3} & \text{if} \quad \text{n} = 3 \end{cases}, \quad \boldsymbol{x} \in \partial\Omega. \tag{3.3}$$

Next, we approximate the displacement vector as

$$\boldsymbol{u}_N(\boldsymbol{x}) = \sum_{\ell=1}^{N} \mathrm{U}(\boldsymbol{x}, \boldsymbol{\xi}_\ell) \, \boldsymbol{d}_\ell + \frac{\overline{\alpha}_T}{2} \left(\frac{1 + \overline{\nu}}{1 - \overline{\nu}} \right) \sum_{\ell=1}^{N} c_\ell \, (\boldsymbol{x} - \boldsymbol{\xi}_\ell) \, F(\boldsymbol{x}, \boldsymbol{\xi}_\ell), \qquad \boldsymbol{x} \in \Omega, \tag{3.4}$$

where $(\boldsymbol{d}_\ell)_{\ell=\overline{1,N}}$ are unknown coefficients and

$$\mathrm{U}(\boldsymbol{x}, \boldsymbol{\xi}) = \begin{cases} \dfrac{1}{8\,\pi\,G(1-\overline{\nu})} \left[-(3 - 4\,\overline{\nu}) \, \log|\boldsymbol{x} - \boldsymbol{\xi}| \, I + \dfrac{(\boldsymbol{x} - \boldsymbol{\xi}) \otimes (\boldsymbol{x} - \boldsymbol{\xi})}{|\boldsymbol{x} - \boldsymbol{\xi}|^2} \right] & \text{if} \quad \text{n} = 2, \\ \\ \dfrac{1}{16\,\pi\,G(1-\overline{\nu})} \left[\dfrac{(3 - 4\,\overline{\nu})}{|\boldsymbol{x} - \boldsymbol{\xi}|} \, I + \dfrac{(\boldsymbol{x} - \boldsymbol{\xi}) \otimes (\boldsymbol{x} - \boldsymbol{\xi})}{|\boldsymbol{x} - \boldsymbol{\xi}|^3} \right] & \text{if} \quad \text{n} = 3, \end{cases} \tag{3.5}$$

are the fundamental solutions of the n = 2− and n = 3−dimensional Lamé system of elasticity.

As boundary collocation points we take $(\boldsymbol{x}_j)_{j=\overline{1,N_1}}$ and $(\boldsymbol{x}_j)_{j=\overline{N_1+1,N}}$ which are uniformly distributed on Γ_1 and Γ_2, respectively. Imposing the boundary conditions (2.7) and (2.8) at these points gives

$$\boldsymbol{u}_N(\boldsymbol{x}_m) = \boldsymbol{f}(\boldsymbol{x}_m), \qquad m = \overline{1,N}, \tag{3.6}$$

and

$$q_N(\boldsymbol{x}_m) = \widetilde{q}(\boldsymbol{x}_m), \qquad m = \overline{1,N_1}, \tag{3.7}$$

where $\boldsymbol{u}_N$ and q_N are given by (3.4) and (3.3), respectively. It remains to impose boundary condition (2.9) which yields:

(i) In n = 2 dimensions, see [16]:

$$\sum_{\ell=1}^{N} \mathrm{T}(\boldsymbol{x}_m,\boldsymbol{\xi}_\ell)\,\boldsymbol{d}_\ell - \frac{\overline{\alpha}_T\,G}{2\,\pi\,\kappa}\left(\frac{1+\overline{\nu}}{1-\overline{\nu}}\right)\sum_{\ell=1}^{N} c_\ell\,\left[\left(-\log|\boldsymbol{x}_m-\boldsymbol{\xi}_\ell| + \frac{\overline{\nu}}{1-2\,\overline{\nu}}\right)\boldsymbol{n}(\boldsymbol{x}_m) + \frac{(\boldsymbol{x}_m-\boldsymbol{\xi}_\ell)\cdot\boldsymbol{n}(\boldsymbol{x}_m)}{|\boldsymbol{x}_m-\boldsymbol{\xi}_\ell|^2}\,(\boldsymbol{x}_m-\boldsymbol{\xi}_\ell)\right]$$
$$= \widetilde{\boldsymbol{t}}(\boldsymbol{x}_m), \quad m = \overline{1,N_1}, \tag{3.8}$$

where T is the two-dimensional fundamental solution for the traction tensor in elasticity given by, see e.g. [2],

$$\mathrm{T}_{1j}(\boldsymbol{x},\boldsymbol{\xi}) = \frac{2\,G}{1-2\,\overline{\nu}}\left[(1-\overline{\nu})\,\frac{\partial \mathrm{U}_{1j}}{\partial x_1}(\boldsymbol{x},\boldsymbol{\xi}) + \overline{\nu}\,\frac{\partial \mathrm{U}_{2j}}{\partial x_2}(\boldsymbol{x},\boldsymbol{\xi})\right] n_1(\boldsymbol{x})$$
$$+G\left[\frac{\partial \mathrm{U}_{1j}}{\partial x_2}(\boldsymbol{x},\boldsymbol{\xi}) + \frac{\partial \mathrm{U}_{2j}}{\partial x_1}(\boldsymbol{x},\boldsymbol{\xi})\right] n_2(\boldsymbol{x}), \quad j = 1,2,$$
$$\mathrm{T}_{2j}(\boldsymbol{x},\boldsymbol{\xi}) = G\left[\frac{\partial \mathrm{U}_{1j}}{\partial x_2}(\boldsymbol{x},\boldsymbol{\xi}) + \frac{\partial \mathrm{U}_{2j}}{\partial x_1}(\boldsymbol{x},\boldsymbol{\xi})\right] n_1(\boldsymbol{x})$$
$$+\frac{2\,G}{1-2\,\overline{\nu}}\left[\overline{\nu}\,\frac{\partial \mathrm{U}_{1j}}{\partial x_1}(\boldsymbol{x},\boldsymbol{\xi}) + (1-\overline{\nu})\,\frac{\partial \mathrm{U}_{2j}}{\partial x_2}(\boldsymbol{x},\boldsymbol{\xi})\right] n_2(\boldsymbol{x}), \quad j = 1,2.$$

(ii) In n = 3 dimensions, see [24]:

$$\sum_{\ell=1}^{N} \mathrm{T}(\boldsymbol{x}_m,\boldsymbol{\xi}_\ell)\,\boldsymbol{d}_\ell - \frac{\overline{\alpha}_T\,G}{4\,\pi\,\kappa}\left(\frac{1+\overline{\nu}}{1-\overline{\nu}}\right)\sum_{\ell=1}^{N} c_\ell\,\left[\left(-\frac{1}{1-2\,\overline{\nu}}\,\frac{1}{|\boldsymbol{x}_m-\boldsymbol{\xi}_\ell|}\right)\boldsymbol{n}(\boldsymbol{x}_m) + \frac{(\boldsymbol{x}_m-\boldsymbol{\xi}_\ell)\cdot\boldsymbol{n}(\boldsymbol{x}_m)}{|\boldsymbol{x}_m-\boldsymbol{\xi}_\ell|^3}(\boldsymbol{x}_m-\boldsymbol{\xi}_\ell)\right]$$
$$= \widetilde{\boldsymbol{t}}(\boldsymbol{x}_m), \quad m = \overline{1,N_1}, \tag{3.9}$$

where T is the three-dimensional fundamental solution for the traction tensor in elasticity given by, see e.g. [2],

$$\mathrm{T}_{1k}(\boldsymbol{x},\boldsymbol{\xi}) = \frac{2\,G}{1-2\,\overline{\nu}}\left[(1-\overline{\nu})\,\frac{\partial \mathrm{U}_{1k}}{\partial x_1}(\boldsymbol{x},\boldsymbol{\xi}) + \overline{\nu}\left(\frac{\partial \mathrm{U}_{2k}}{\partial x_2}(\boldsymbol{x},\boldsymbol{\xi}) + \frac{\partial \mathrm{U}_{3k}}{\partial x_3}(\boldsymbol{x},\boldsymbol{\xi})\right)\right] n_1(\boldsymbol{x})$$
$$+G\left[\frac{\partial \mathrm{U}_{1k}}{\partial x_2}(\boldsymbol{x},\boldsymbol{\xi}) + \frac{\partial \mathrm{U}_{2k}}{\partial x_1}(\boldsymbol{x},\boldsymbol{\xi})\right] n_2(\boldsymbol{x}) + G\left[\frac{\partial \mathrm{U}_{1k}}{\partial x_3}(\boldsymbol{x},\boldsymbol{\xi}) + \frac{\partial \mathrm{U}_{3k}}{\partial x_1}(\boldsymbol{x},\boldsymbol{\xi})\right] n_3(\boldsymbol{x}), \quad k = 1,2,3,$$
$$\mathrm{T}_{2k}(\boldsymbol{x},\boldsymbol{\xi}) = \frac{2\,G}{1-2\,\overline{\nu}}\left[(1-\overline{\nu})\frac{\partial \mathrm{U}_{2k}}{\partial x_2}(\boldsymbol{x},\boldsymbol{\xi}) + \overline{\nu}\left(\frac{\partial \mathrm{U}_{3k}}{\partial x_3}(\boldsymbol{x},\boldsymbol{\xi}) + \frac{\partial \mathrm{U}_{1k}}{\partial x_1}(\boldsymbol{x},\boldsymbol{\xi})\right)\right] n_2(\boldsymbol{x})$$
$$+G\left[\frac{\partial \mathrm{U}_{2k}}{\partial x_3}(\boldsymbol{x},\boldsymbol{\xi}) + \frac{\partial \mathrm{U}_{3k}}{\partial x_2}(\boldsymbol{x},\boldsymbol{\xi})\right] n_3(\boldsymbol{x}) + G\left[\frac{\partial \mathrm{U}_{2k}}{\partial x_1}(\boldsymbol{x},\boldsymbol{\xi}) + \frac{\partial \mathrm{U}_{1k}}{\partial x_2}(\boldsymbol{x},\boldsymbol{\xi})\right] n_1(\boldsymbol{x}), \quad k = 1,2,3,$$
$$\mathrm{T}_{3k}(\boldsymbol{x},\boldsymbol{\xi}) = \frac{2\,G}{1-2\,\overline{\nu}}\left[(1-\overline{\nu})\frac{\partial \mathrm{U}_{3k}}{\partial x_3}(\boldsymbol{x},\boldsymbol{\xi}) + \overline{\nu}\left(\frac{\partial \mathrm{U}_{1k}}{\partial x_1}(\boldsymbol{x},\boldsymbol{\xi}) + \frac{\partial \mathrm{U}_{2k}}{\partial x_2}(\boldsymbol{x},\boldsymbol{\xi})\right)\right] n_3(\boldsymbol{x})$$
$$+G\left[\frac{\partial \mathrm{U}_{3k}}{\partial x_1}(\boldsymbol{x},\boldsymbol{\xi}) + \frac{\partial \mathrm{U}_{1k}}{\partial x_3}(\boldsymbol{x},\boldsymbol{\xi})\right] n_1(\boldsymbol{x}) + G\left[\frac{\partial \mathrm{U}_{3k}}{\partial x_2}(\boldsymbol{x},\boldsymbol{\xi}) + \frac{\partial \mathrm{U}_{2k}}{\partial x_3}(\boldsymbol{x},\boldsymbol{\xi})\right] n_2(\boldsymbol{x}), \quad k = 1,2,3.$$

The systems of equations (3.6), (3.7) and (3.8) or (3.9) consist of $(\mathrm{n}+1)N_1+\mathrm{n}N$ linear equations in $(\mathrm{n}+1)N$ unknowns, and we thus require that $(\mathrm{n}+1)N_1 \geq N$. We write these linear systems of equations in the generic form

$$A\,\mathbf{x} = \mathbf{f}, \tag{3.10}$$

where A is the matrix with $(\mathrm{n}+1)N_1+\mathrm{n}N$ rows and $(\mathrm{n}+1)N$ columns, $\mathbf{f}$ is a known right-hand side vector given by

$$\mathbf{f} = \left[\left(\boldsymbol{f}(\boldsymbol{x}_m)\right)_{m=\overline{1,N}}, \left(\widetilde{q}(\boldsymbol{x}_m)\right)_{m=\overline{1,N_1}}, \left(\widetilde{\boldsymbol{t}}(\boldsymbol{x}_m)\right)_{m=\overline{1,N_1}} \right]^{\mathrm{T}} \tag{3.11}$$

and $\mathbf{x}$ is the desired solution containing the vector of MFS coefficients, namely,

$$\mathbf{x} = \left[\left(\boldsymbol{d}_\ell\right)_{\ell=\overline{1,N}}, \left(c_\ell\right)_{\ell=\overline{1,N}} \right]^{\mathrm{T}}. \tag{3.12}$$

Since the inverse problem under consideration is ill-posed, the resulting system of equations (3.10) is ill-conditioned, and in order to obtain a stable solution we employ the TRM [14, Chapter 4.4], see also, [25, Chapter 5] which yields the solution

$$\mathbf{x}_\lambda = \left(A^{\mathrm{T}}A + \lambda \mathrm{I}\right)^{-1} A^{\mathrm{T}}\mathbf{f}, \tag{3.13}$$

where $\lambda > 0$ is a regularization parameter to be prescribed and I is the identity matrix of order $(\mathrm{n}+1)N$. In this paper, we choose the regularization parameter at the corner of the L-curve obtained by plotting the residual norm, $\|A\mathbf{x}-\mathbf{f}\|_2$, versus the solution norm, $\|\mathbf{x}\|_2$ for many positive values of λ, see [14, Chapter 4.7] or [25, Chapter 5.4.2].

Other regularization methods based on the singular value decomposition (SVD) [14, Chapter 3.2], see also, [25, Chapter 4], as well as other criteria for choosing the regularization parameter, e.g. the discrepancy principle or the generalized cross validation can be employed, see [23, 24].

One can also remark that the unknowns $\left(\boldsymbol{d}_\ell\right)_{\ell=\overline{1,N}}$ and $\left(c_\ell\right)_{\ell=\overline{1,N}}$ in the vector $\mathbf{x}$ in (3.12) represent the intensities of the fictitious point forces in (3.4) and heat sources in (3.1), respectively. Consequently, they represent different physical quantities and may have different orders of magnitude. Some scaling for normalization could potentially be used for the different components of the vector $\mathbf{x}$. However, the inaccuracies observed in some of the results presented in the next section are not due to the MFS discretization but to the added noise in the input data. Hence, the normalization of the components of vector $\mathbf{x}$ did not seem necessary. On the other hand, one could use different regularization parameters, i.e. replace $\lambda\mathrm{I}$ in (3.13) by a diagonal matrix whose first $\mathrm{n}N$ entries are equal to $\lambda_1 > 0$ and its last N entries are equal to $\lambda_2 > 0$. In this case, however, one would have to choose two regularization parameters λ_1 and λ_2 using, for example, the L-surface method [5], which would render the investigation considerably more complicated and tedious.

4. Numerical examples

Throughout this section the material constants were taken to be as follows: $G = 4.8\times10^{10}\mathrm{N/m}^2$, $\nu = 0.34$, $\kappa = 4.01\mathrm{Wm}^{-1}\mathrm{K}^{-1}$ and $\alpha_T = 16.5\times10^{-6}\ {}^\circ\mathrm{C}^{-1}$. For simplicity, we consider only the case of plane strain thermoelasticity, where $\overline{\nu} = \nu$ and $\overline{\alpha}_T = \alpha_T$.

For any real-valued function $g : \Gamma \longrightarrow \mathbb{R}$, where $\Gamma = \Gamma_2$ or $\Gamma = \partial\Omega$, and any set of points $\left\{\boldsymbol{x}^{(n)}\right\}_{n=\overline{1,N_\Gamma}} \subset \Gamma$, we introduce the following *relative root mean square (RMS) error* of g on Γ:

$$\mathrm{e}_\Gamma(g) = \sqrt{\frac{1}{N_\Gamma}\sum_{n=1}^{N_\Gamma}\left[g^{(\mathrm{num})}\left(\boldsymbol{x}^{(n)}\right) - g\left(\boldsymbol{x}^{(n)}\right)\right]^2} \Bigg/ \sqrt{\frac{1}{N_\Gamma}\sum_{n=1}^{N_\Gamma} g\left(\boldsymbol{x}^{(n)}\right)^2}\ , \tag{4.1a}$$

where $g^{(\mathrm{num})}(\boldsymbol{x})$ denotes an approximate numerical value for $g(\boldsymbol{x})$, $\boldsymbol{x}\in\Gamma$. To investigate the local accuracy of the numerical solution, one could also employ the following *pointwise normalized error* of g at $\boldsymbol{x}^{(n)}\in\Gamma$:

$$\mathrm{E}_g(\boldsymbol{x}^{(n)})=\frac{\left|g^{(\mathrm{num})}(\boldsymbol{x}^{(n)})-g(\boldsymbol{x}^{(n)})\right|}{\max_{m=\overline{1,N_\Gamma}}\left|g(\boldsymbol{x}^{(m)})\right|},\quad n=\overline{1,N_\Gamma}\,. \tag{4.1b}$$

Stability is numerically investigated by inverting the data (2.8), and (2.7) and (2.9), the latter two contaminated with noise as $\boldsymbol{f}(1+p_{\boldsymbol{u}}\varrho)$ and $\widetilde{\boldsymbol{t}}(1+p_{\boldsymbol{t}}\varrho)$, respectively, where $p_{\boldsymbol{u}}$ and $p_{\boldsymbol{t}}$ represent the percentage of noise and ϱ is a random variable drawn from a uniform distribution in [-1, 1].

4.1. **Example 1.** (n=2-dimensions). We first consider an example in the unit disk (radius 1m) with exact solution

$$T(\boldsymbol{x})=100\log|\boldsymbol{x}-\boldsymbol{x}_0|,\quad \boldsymbol{u}(\boldsymbol{x})=\frac{\alpha_T}{2}\left(\frac{1+\nu}{1-\nu}\right)T(\boldsymbol{x})(\boldsymbol{x}-\boldsymbol{x}_0),\quad \text{where}\quad \boldsymbol{x}_0=(8,1), \tag{4.2}$$

in $\Omega=B(\mathbf{0};1)$ and $\Gamma_1=\{(\cos\vartheta,\sin\vartheta),0\le\vartheta\le\alpha\pi\}$.

We investigate three cases when $\alpha\in\{2/3,1,4/3\}$ corresponding, in terms of the length of the boundary on which the data (2.8) and (2.9) are supplemented, to under-determined, determined and over-determined data, i.e. $|\Gamma_1|/|\Gamma_2|\in\{1/2,1,2\}$, respectively. However, if we take $N_1=\alpha N/2$, then for all these values of α the condition $N\le(\mathrm{n}+1)N_1=3N_1=3\alpha N/2$ is always satisfied and the system of linear equations (3.6)-(3.8) has at least as many equations as unknowns. We take the MFS parameters to be $N=84, N_1=\alpha N/2$ and the sources are placed on an exterior disk of radius $1+d$, where $d=4$. Other values of d can be chosen, but once d increases beyond a threshold where an exterior singularity in the solution occurs, the numerical results may begin to deteriorate and instability may appear. It is therefore recommended to start with a small value of d and increase it gradually until a possible blow-up occurs. For more details regarding such issues in the MFS, see, e.g. [4, 6].

In Figures 1, 3 and 5 the numerical results for $T|_{\partial\Omega}$, $q|_{\Gamma_2}$ and $\boldsymbol{t}|_{\Gamma_2}$ are compared to the corresponding analytical solutions for various percentages of noise $p_{\boldsymbol{u}}=p_{\boldsymbol{t}}\in\{1,3,5\}\%$, when $\alpha=4/3$, $\alpha=1$ and $\alpha=2/3$, respectively, obtained using the MFS and TRM with the choice of the regularization parameter based on the L-curve criterion as illustrated in Figures 2, 4 and 6. We also report that the least squares numerical results with no regularization, i.e. $\lambda=0$ in (3.13) were highly oscillatory and unbounded giving rise to unstable solutions and are therefore not presented.

First, from Figures 2, 4 and 6 one may observe that L-curves with well-defined corners occur in all cases investigated, thus providing an appropriate approximate value for the regularization parameter λ in (3.13).

Secondly, Figures 1, 3 and 5 reveal that:

(i) The heat flux $q|_{\Gamma_2}$ is very accurately retrieved, almost independently of the percentage of noise $p_{\boldsymbol{u}}=p_{\boldsymbol{t}}$ and the values of α.
(ii) The temperature $T|_{\partial\Omega}$ is stable and becomes more accurate as the percentage of noise decreases. The prediction is also not significantly dependent on α.
(iii) The traction components, especially t_1, are significantly affected by the presence of noise and their accuracy and stability depend considerably on the length over which the data (2.8) and (2.9) is prescribed.

4.2. **Example 2.** (n=3-dimensions). The second, three-dimensional, example is in the unit sphere (radius 1m) with exact solution

$$T(\boldsymbol{x})=\frac{T_1}{|\boldsymbol{x}-\boldsymbol{x}^{(1)}|}+\frac{T_2}{|\boldsymbol{x}-\boldsymbol{x}^{(2)}|},\qquad \boldsymbol{u}(\boldsymbol{x})=\frac{\alpha_{\mathrm{T}}}{2}\left(\frac{1+\nu}{1-\nu}\right)\left[T_1\frac{(\boldsymbol{x}-\boldsymbol{x}^{(1)})}{|\boldsymbol{x}-\boldsymbol{x}^{(1)}|}+T_2\frac{(\boldsymbol{x}-\boldsymbol{x}^{(2)})}{|\boldsymbol{x}-\boldsymbol{x}^{(2)}|}\right], \tag{4.3}$$

where $T_1=2000°\mathrm{C}$, $T_2=-500°\mathrm{C}$, $\boldsymbol{x}^{(1)}=(5,5,5)$, $\boldsymbol{x}^{(2)}=(-2,4,4)$, and
$\Gamma_1=\{(\cos\vartheta\sin\phi,\sin\vartheta\sin\phi,\cos\phi),\vartheta\in[0,2\pi),0\le\phi\le\pi/2\}$. For simplicity, we only consider the determined situation in which $|\Gamma_1|=|\Gamma_2|$.

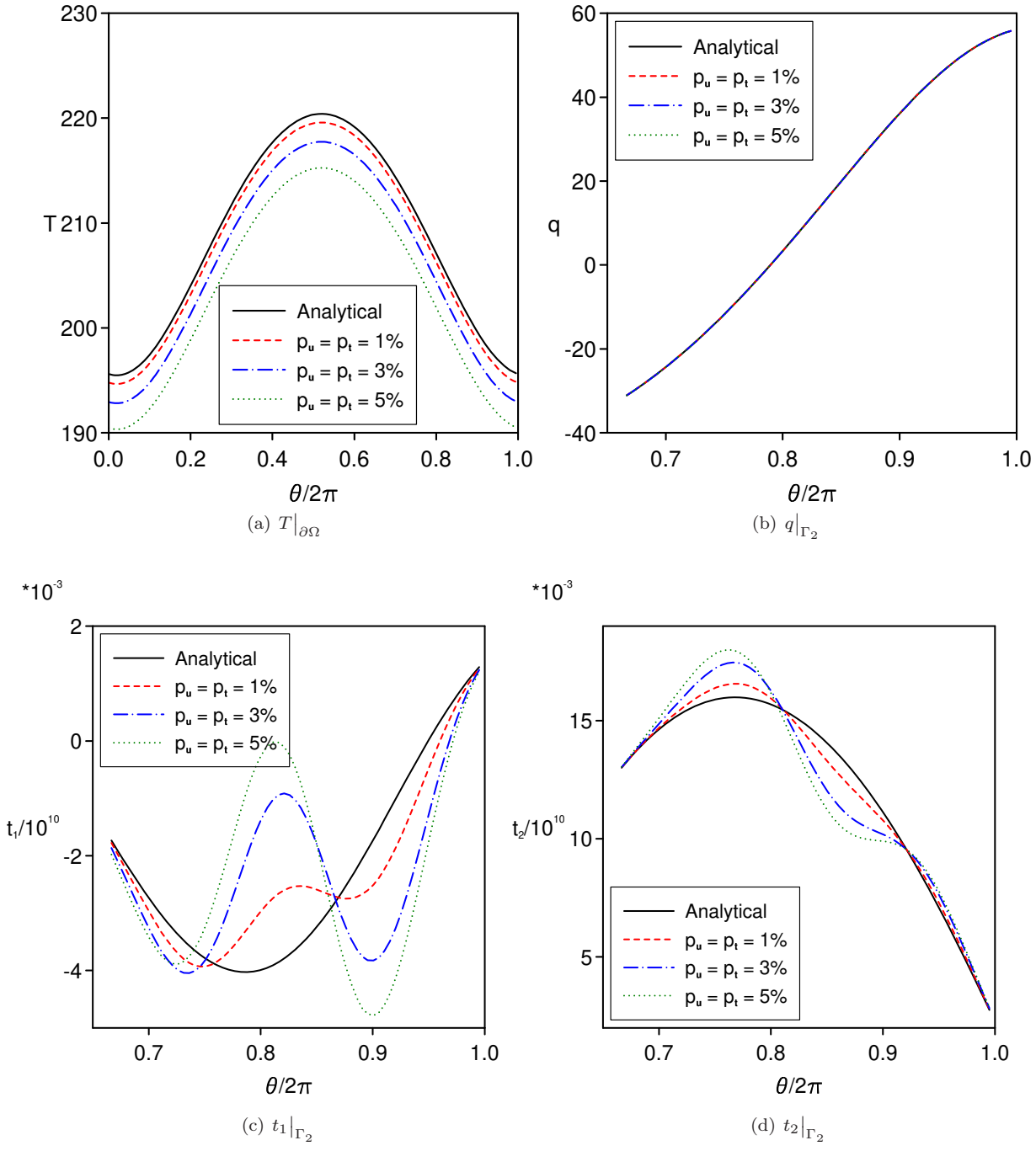

(a) $T\big|_{\partial\Omega}$ (b) $q\big|_{\Gamma_2}$

(c) $t_1\big|_{\Gamma_2}$ (d) $t_2\big|_{\Gamma_2}$

FIGURE 1. Example 1: The analytical and numerical (a) temperature $T\big|_{\partial\Omega}$ (in °C), (b) heat flux $q\big|_{\Gamma_2}$ (in Wm^{-2}), (c) traction $t_1\big|_{\Gamma_2}$ (in Nm^{-2}), and (d) traction $t_2\big|_{\Gamma_2}$ (in Nm^{-2}), when $\alpha = 4/3$.

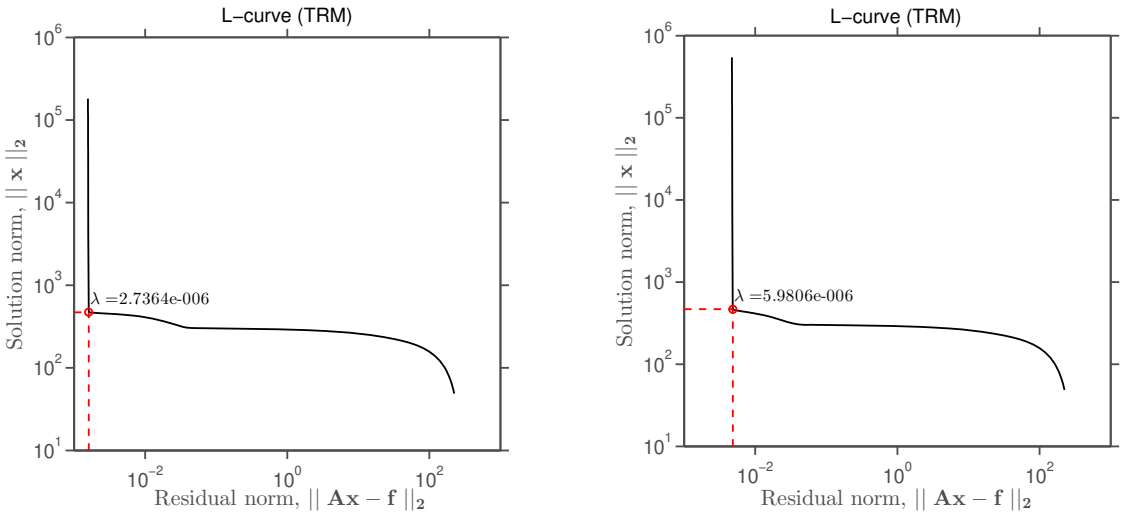

(a) $p_{\boldsymbol{u}} = p_{\boldsymbol{t}} = 1\%$ (b) $p_{\boldsymbol{u}} = p_{\boldsymbol{t}} = 3\%$

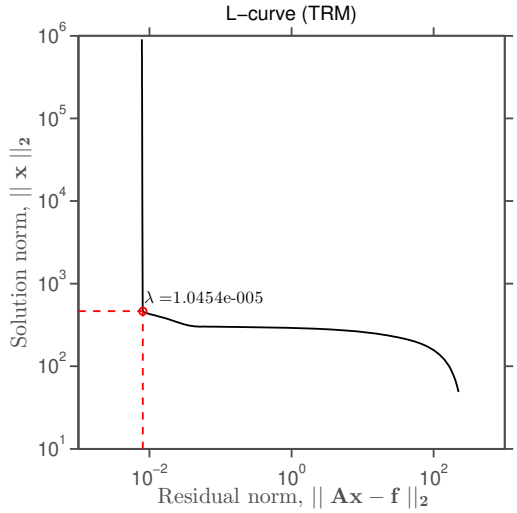

(c) $p_{\boldsymbol{u}} = p_{\boldsymbol{t}} = 5\%$

FIGURE 2. Example 1: The L-curves for various percentages of noise $p_{\boldsymbol{u}} = p_{\boldsymbol{t}} \in \{1, 3, 5\}\%$, when $\alpha = 4/3$.

The MFS parameters are taken to be $N = 840, N_1 = 420$ and the sources are placed on an exterior sphere of radius $1 + d$, where $d = 4$. Figures 7 and 8 show the analytical and numerical solutions for the temperature on $\partial\Omega$, the heat flux on Γ_2 and the components t_1 and t_3 of the traction on Γ_2, respectively, obtained using the MFS and TRM with the choice of the regularization parameters given by the regularization parameters given by the L-curves illustrated in Figure 11 for various percentages of noise. For brevity, the results for the component t_2 are not presented. From these figures it can be observed that there is very good agreement between the analytical and numerical solutions. Better quantification of the errors can be seen from Figures 9 and 10 where the pointwise

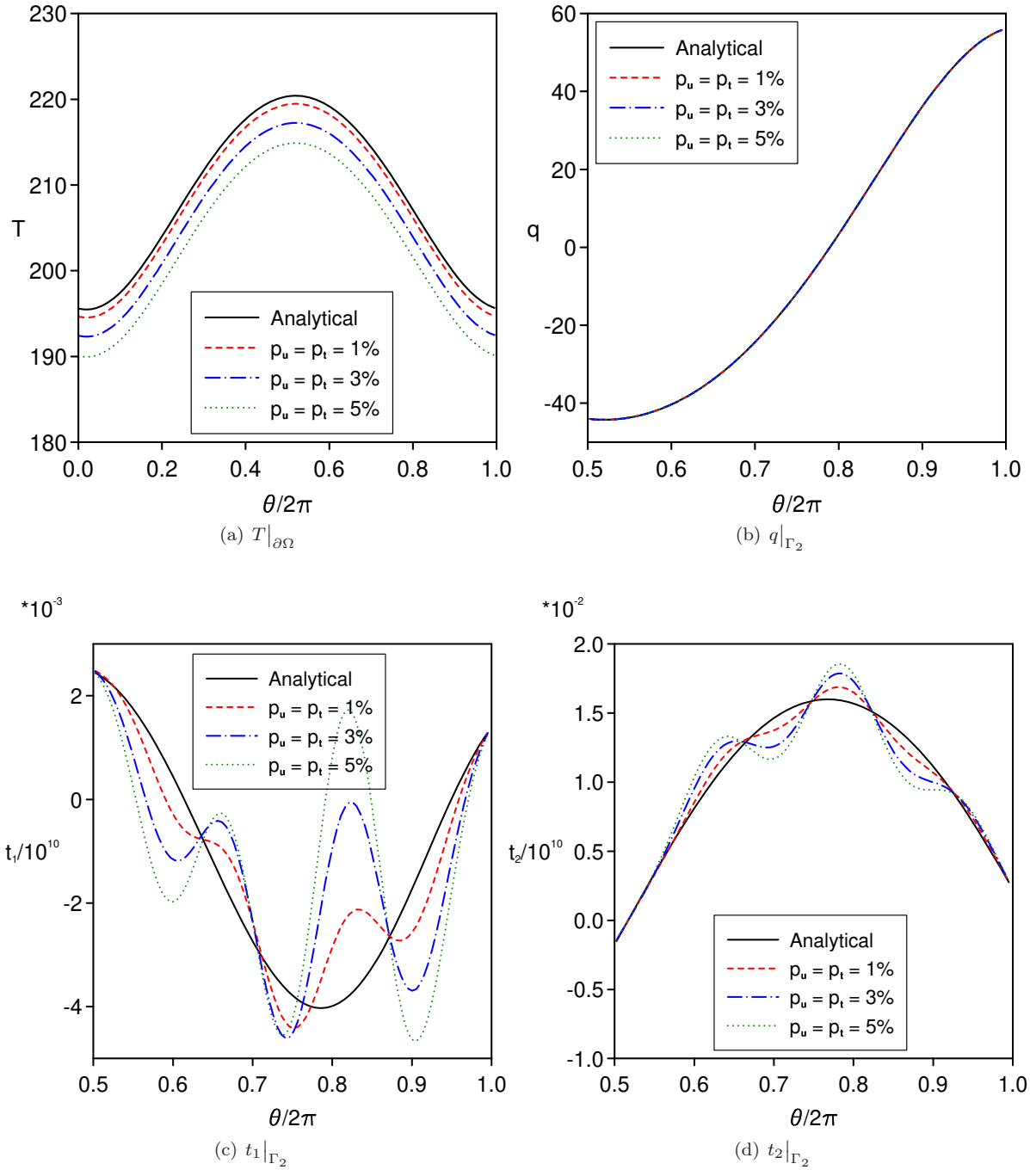

(a) $T\big|_{\partial\Omega}$ (b) $q\big|_{\Gamma_2}$

(c) $t_1\big|_{\Gamma_2}$ (d) $t_2\big|_{\Gamma_2}$

FIGURE 3. Example 1: The analytical and numerical (a) temperature $T\big|_{\partial\Omega}$ (in °C), (b) heat flux $q\big|_{\Gamma_2}$ (in Wm^{-2}), (c) traction $t_1\big|_{\Gamma_2}$ (in Nm^{-2}), and (d) traction $t_2\big|_{\Gamma_2}$ (in Nm^{-2}), when $\alpha = 1$.

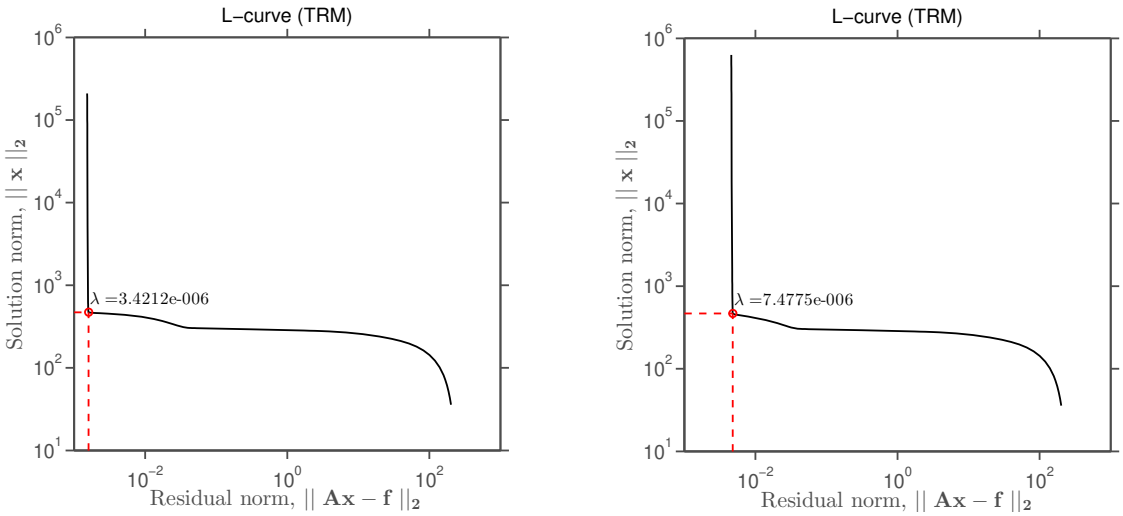

(a) $p_{\boldsymbol{u}} = p_{\boldsymbol{t}} = 1\%$ (b) $p_{\boldsymbol{u}} = p_{\boldsymbol{t}} = 3\%$

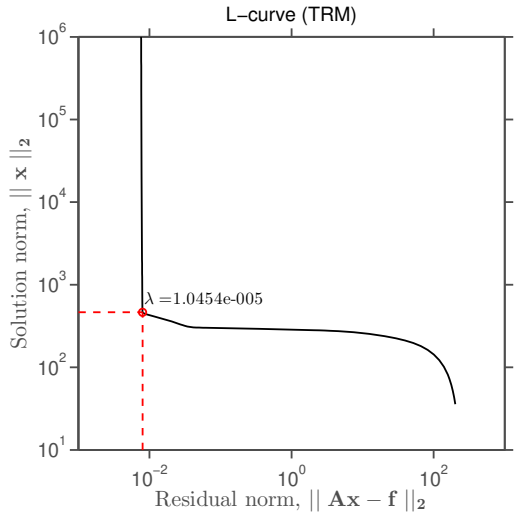

(c) $p_{\boldsymbol{u}} = p_{\boldsymbol{t}} = 5\%$

FIGURE 4. Example 1: The L-curves for various percentages of noise $p_{\boldsymbol{u}} = p_{\boldsymbol{t}} \in \{1, 3, 5\}\%$, when $\alpha = 1$.

normalized errors (4.1b) for $\mathrm{E}_T|_{\partial\Omega}$, $\mathrm{E}_q|_{\Gamma_2}$, $\mathrm{E}_{t_1}|_{\Gamma_2}$ and $\mathrm{E}_{t_3}|_{\Gamma_2}$, respectively, are illustrated. From these figures it can be seen that the errors are comparable with the amount of noise with which the input data (2.7) and (2.9) are contaminated. Also, the errors decrease as the amount of noise decreases. This shows that stable solutions have been achieved.

We conclude this section with a brief discussion of the choice of the regularization parameters λ given by the corners of the L-curves plotted in Figures 2, 4, 6 and 11 and, for more clarity, tabulated in Table 1 for various percentages of noise $p_{\boldsymbol{u}} = p_{\boldsymbol{t}} \in \{1, 3, 5\}\%$ for Examples 1 and 2. From this table it can be observed that that the regularization

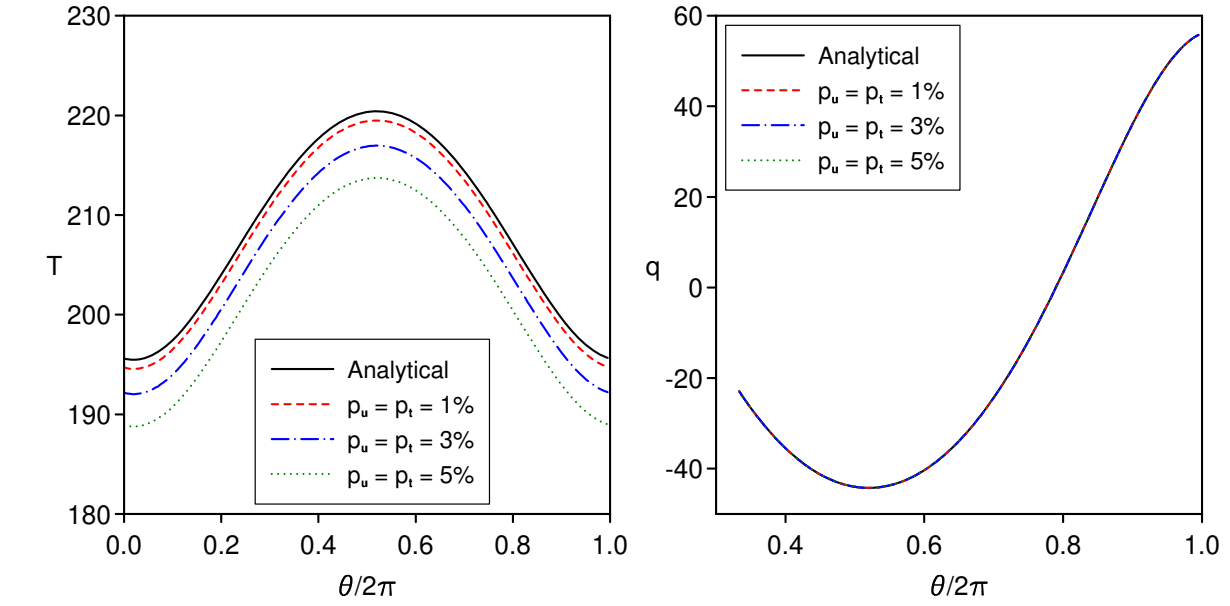

(a) $T\big|_{\partial\Omega}$ (b) $q\big|_{\Gamma_2}$

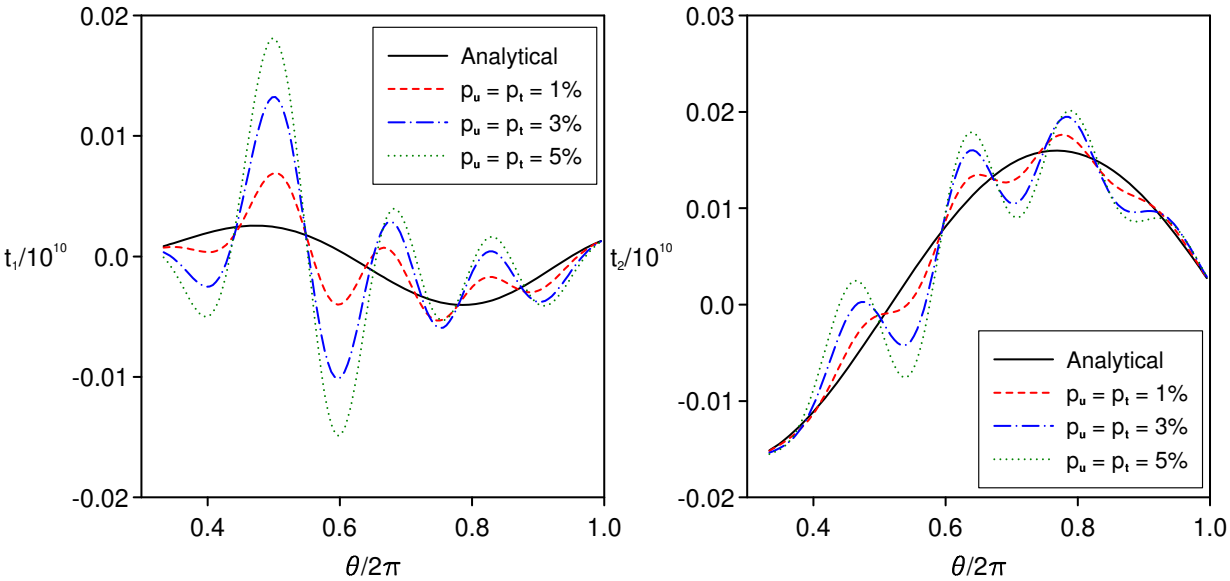

(c) $t_1\big|_{\Gamma_2}$ (d) $t_2\big|_{\Gamma_2}$

FIGURE 5. Example 1: The analytical and numerical (a) temperature $T\big|_{\partial\Omega}$ (in °C), (b) heat flux $q\big|_{\Gamma_2}$ (in Wm^{-2}), (c) traction $t_1\big|_{\Gamma_2}$ (in Nm^{-2}), and (d) traction $t_2\big|_{\Gamma_2}$ (in Nm^{-2}), when $\alpha = 2/3$.

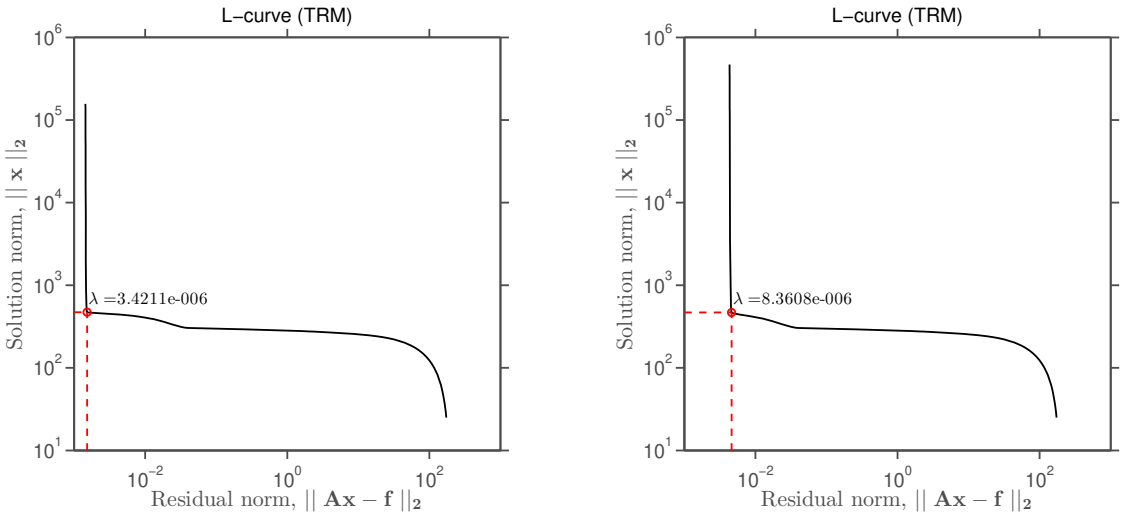

(a) $p_{\boldsymbol{u}} = p_{\boldsymbol{t}} = 1\%$ (b) $p_{\boldsymbol{u}} = p_{\boldsymbol{t}} = 3\%$

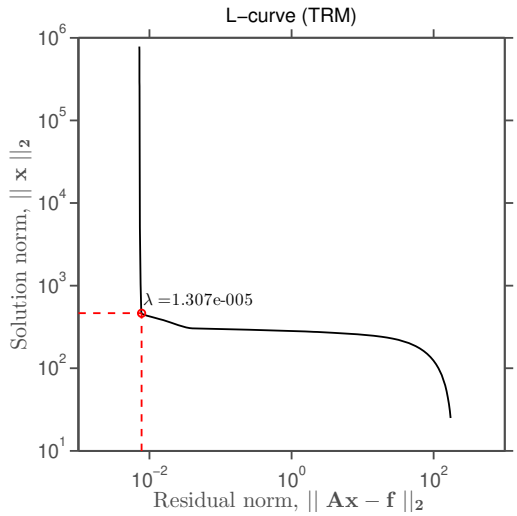

(c) $p_{\boldsymbol{u}} = p_{\boldsymbol{t}} = 5\%$

FIGURE 6. Example 1: The L-curves for various percentages of noise $p_{\boldsymbol{u}} = p_{\boldsymbol{t}} \in \{1, 3, 5\}\%$, when $\alpha = 2/3$.

parameter $\lambda > 0$ depends on the amount of noise, as it should [3], and, as expected, it increases as the amount of noise increases. Also, the larger the portion of the data provided the less ill-posed the problem, hence a smaller regularization parameter is required.

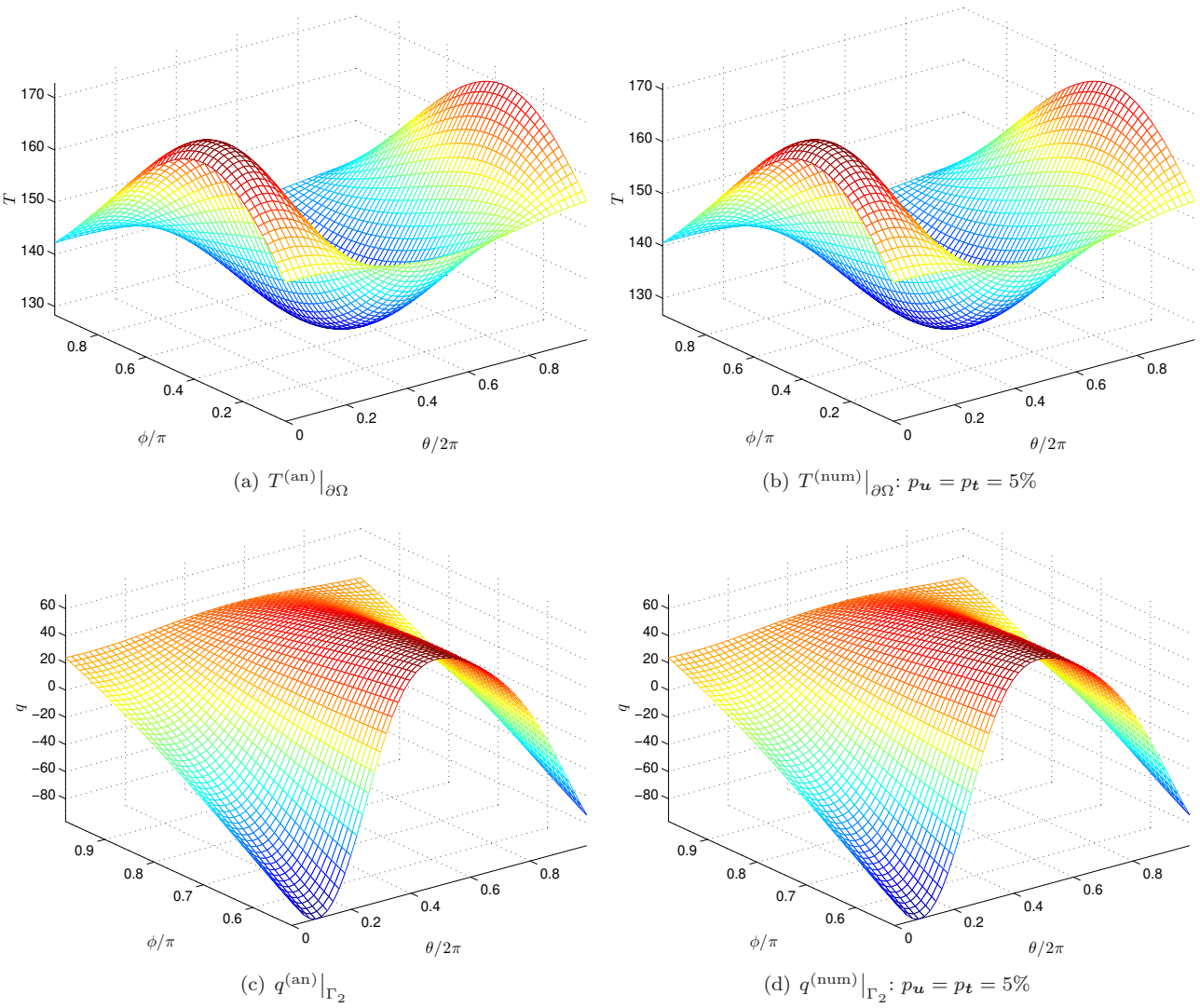

(a) $T^{(\mathrm{an})}\big|_{\partial\Omega}$ (b) $T^{(\mathrm{num})}\big|_{\partial\Omega}$: $p_{\boldsymbol{u}} = p_{\boldsymbol{t}} = 5\%$

(c) $q^{(\mathrm{an})}\big|_{\Gamma_2}$ (d) $q^{(\mathrm{num})}\big|_{\Gamma_2}$: $p_{\boldsymbol{u}} = p_{\boldsymbol{t}} = 5\%$

FIGURE 7. Example 2: The (a) analytical $T^{(\mathrm{an})}\big|_{\partial\Omega}$ (in °C), (b) numerical temperature $T^{(\mathrm{num})}\big|_{\partial\Omega}$ (in °C), (c) analytical $q^{(\mathrm{an})}\big|_{\Gamma_2}$ (in Wm^{-2}), and (d) numerical heat flux $q^{(\mathrm{num})}\big|_{\Gamma_2}$ (in Wm^{-2}), for $p_{\boldsymbol{u}} = p_{\boldsymbol{t}} =5\%$ noise.

5. CONCLUSIONS

In this paper, a new inverse problem in static linear thermo-elasticity is investigated both theoretically, with the uniqueness of the solution being established, and numerically. The problem is ill-posed since small errors in the input data lead to large errors in the output solution. In order to restore stability, the TRM has been employed with the choice of the regularization parameter based on the L-curve criterion. The numerical results obtained for both two- and three-dimensional problems show that the present technique leads to accurate and stable numerical solutions.

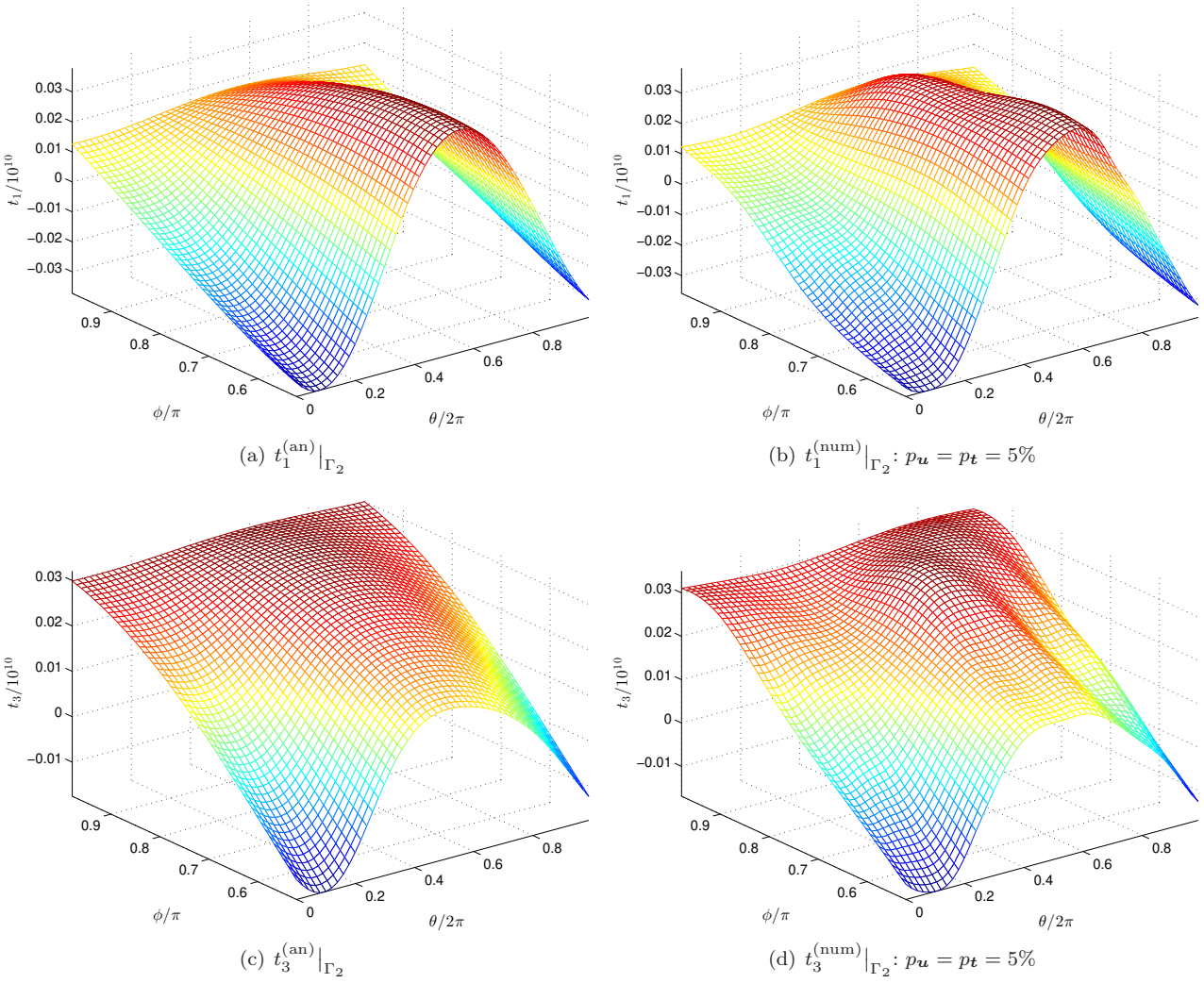

(a) $t_1^{(\mathrm{an})}\big|_{\Gamma_2}$ (b) $t_1^{(\mathrm{num})}\big|_{\Gamma_2}$: $p_{\boldsymbol{u}} = p_{\boldsymbol{t}} = 5\%$

(c) $t_3^{(\mathrm{an})}\big|_{\Gamma_2}$ (d) $t_3^{(\mathrm{num})}\big|_{\Gamma_2}$: $p_{\boldsymbol{u}} = p_{\boldsymbol{t}} = 5\%$

FIGURE 8. Example 2: The (a) analytical $t_1^{(\mathrm{an})}\big|_{\Gamma_2}$ (in Nm^{-2}), (b) numerical traction $t_1^{(\mathrm{num})}\big|_{\Gamma_2}$ (in Nm^{-2}), (c) analytical $t_3^{(\mathrm{an})}\big|_{\Gamma_2}$ (in Nm^{-2}), and (d) numerical traction $t_3^{(\mathrm{num})}\big|_{\Gamma_2}$ (in Nm^{-2}), for $p_{\boldsymbol{u}} = p_{\boldsymbol{t}} = 5\%$ noise.

In conclusion, we believe that our contribution has enlarged the sphere of analysis of separate thermal and elastic inverse problems to the joint thermo-elastic field. This extension can be further enlarged by coupling the thermo-elastic and magnetic fields, see [11], but the numerical investigation of such inverse magneto-thermo-elastic problems is deferred to future work.

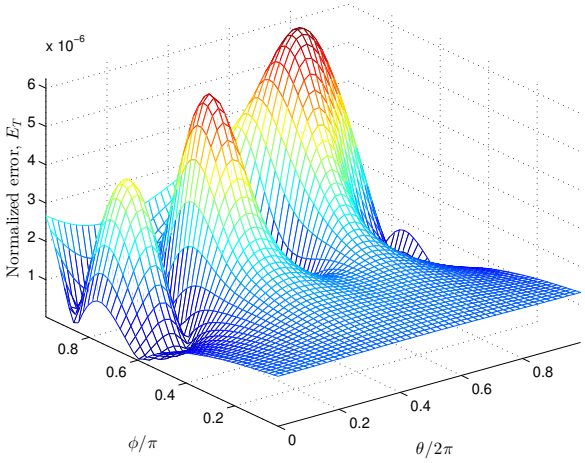

(a) $\mathrm{E}_T\big|_{\partial\Omega}$: $p_{\boldsymbol{u}} = p_{\boldsymbol{t}} = 1\%$

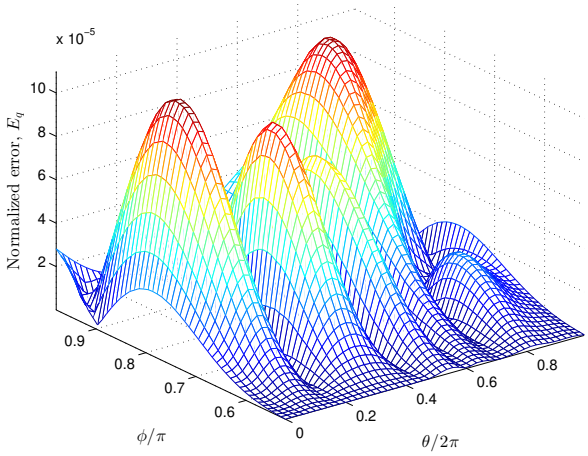

(b) $\mathrm{E}_q\big|_{\Gamma_2}$: $p_{\boldsymbol{u}} = p_{\boldsymbol{t}} = 1\%$

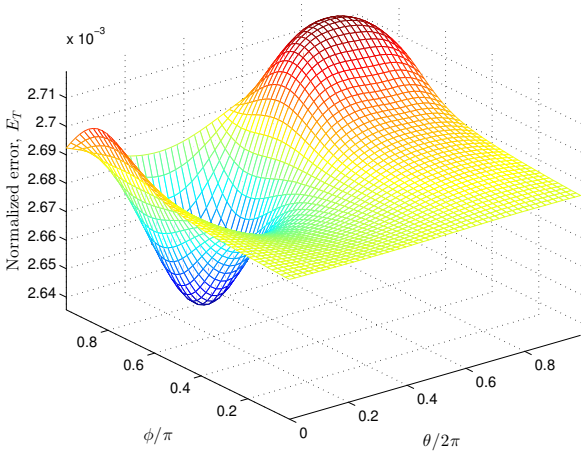

(c) $\mathrm{E}_T\big|_{\partial\Omega}$: $p_{\boldsymbol{u}} = p_{\boldsymbol{t}} = 3\%$

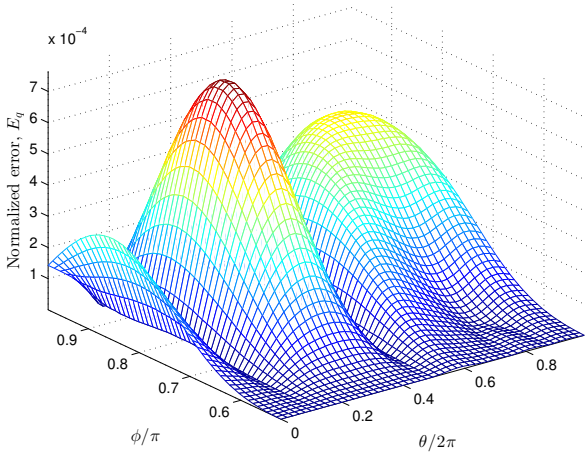

(d) $\mathrm{E}_q\big|_{\Gamma_2}$: $p_{\boldsymbol{u}} = p_{\boldsymbol{t}} = 3\%$

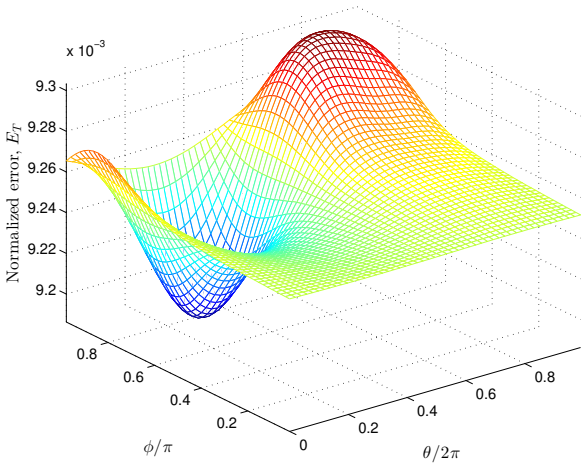

(e) $\mathrm{E}_T\big|_{\partial\Omega}$: $p_{\boldsymbol{u}} = p_{\boldsymbol{t}} = 5\%$

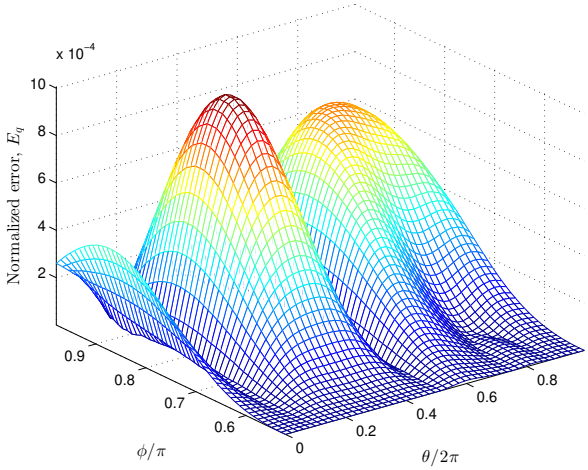

(f) $\mathrm{E}_q\big|_{\Gamma_2}$: $p_{\boldsymbol{u}} = p_{\boldsymbol{t}} = 5\%$

FIGURE 9. Example 2: The normalized errors (a), (c), and (e) $\mathrm{E}_T\big|_{\partial\Omega}$, and (b), (d), and (f) $\mathrm{E}_q\big|_{\Gamma_2}$, for various percentages of noise $p_{\boldsymbol{u}} = p_{\boldsymbol{t}} \in \{1, 3, 5\}\%$.

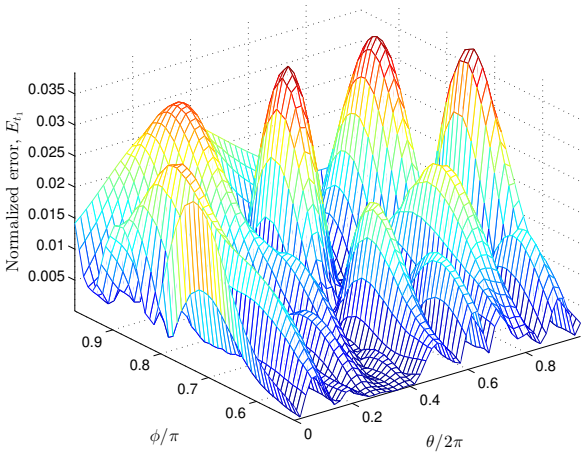

(a) $\mathrm{E}_{t_1}\big|_{\Gamma_2}$: $p_{\boldsymbol{u}} = p_{\boldsymbol{t}} = 1\%$

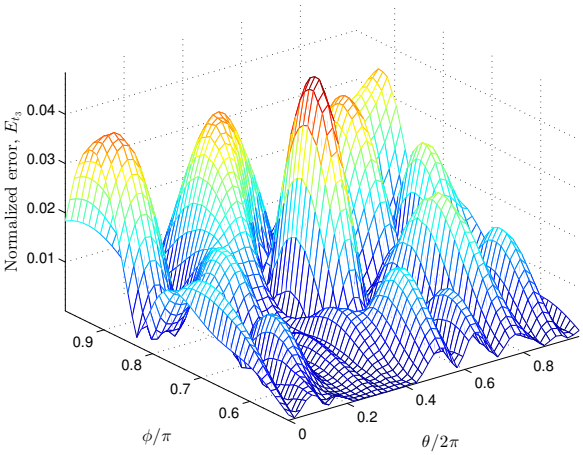

(b) $\mathrm{E}_{t_3}\big|_{\Gamma_2}$: $p_{\boldsymbol{u}} = p_{\boldsymbol{t}} = 1\%$

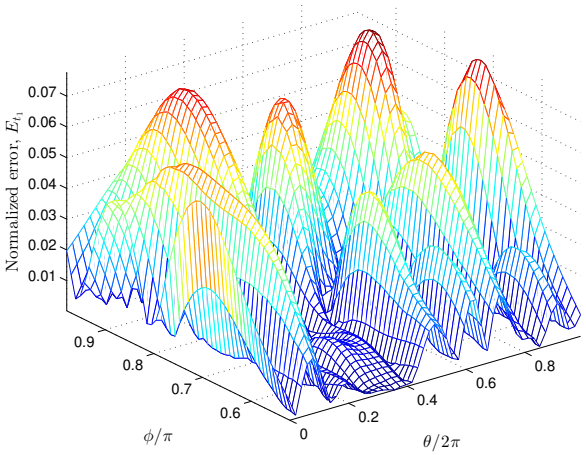

(c) $\mathrm{E}_{t_1}\big|_{\Gamma_2}$: $p_{\boldsymbol{u}} = p_{\boldsymbol{t}} = 3\%$

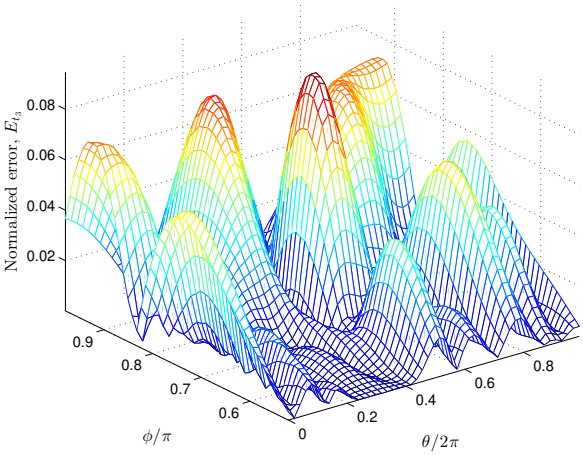

(d) $\mathrm{E}_{t_3}\big|_{\Gamma_2}$: $p_{\boldsymbol{u}} = p_{\boldsymbol{t}} = 3\%$

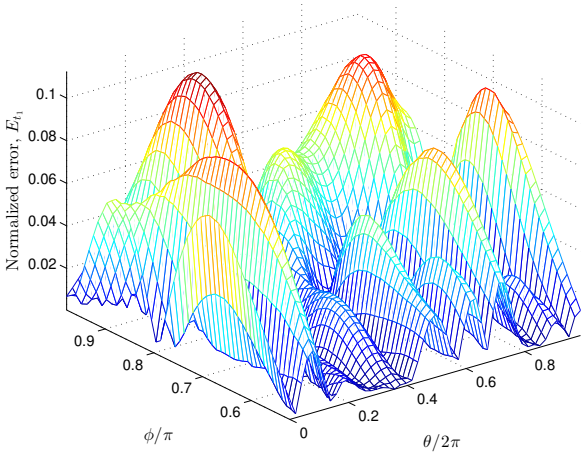

(e) $\mathrm{E}_{t_1}\big|_{\Gamma_2}$: $p_{\boldsymbol{u}} = p_{\boldsymbol{t}} = 5\%$

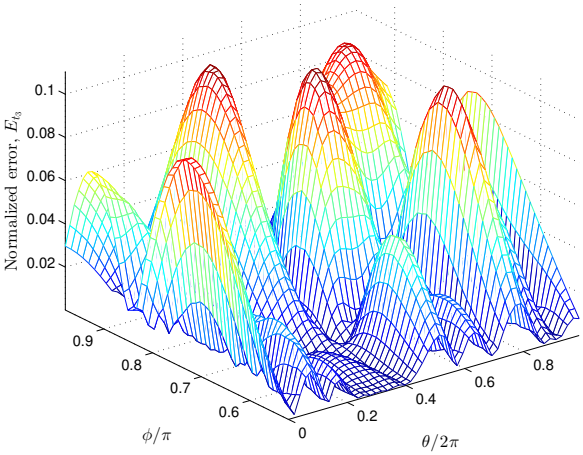

(f) $\mathrm{E}_{t_3}\big|_{\Gamma_2}$: $p_{\boldsymbol{u}} = p_{\boldsymbol{t}} = 5\%$

FIGURE 10. Example 2: The normalized errors (a), (c), and (e) $\mathrm{E}_{t_1}\big|_{\Gamma_2}$, and (b), (d), and (f) $\mathrm{E}_{t_3}\big|_{\Gamma_2}$, for various percentages of noise $p_{\boldsymbol{u}} = p_{\boldsymbol{t}} \in \{1, 3, 5\}\%$.

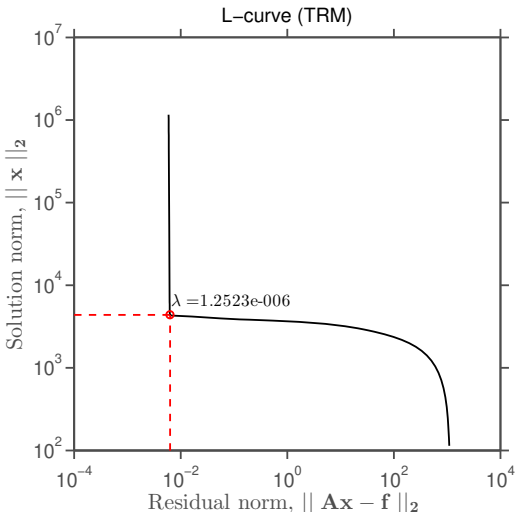

(a) $p_{\boldsymbol{u}} = p_{\boldsymbol{t}} = 1\%$

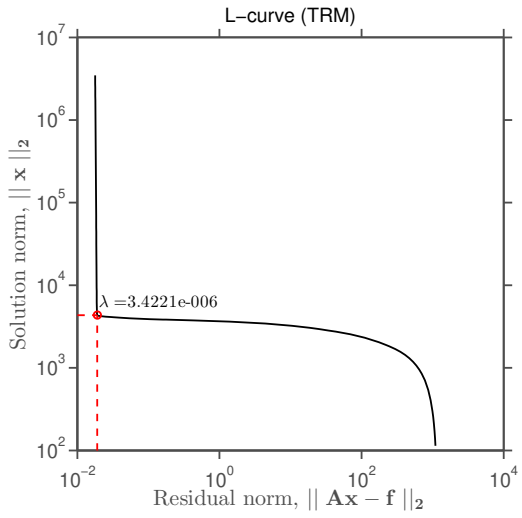

(b) $p_{\boldsymbol{u}} = p_{\boldsymbol{t}} = 3\%$

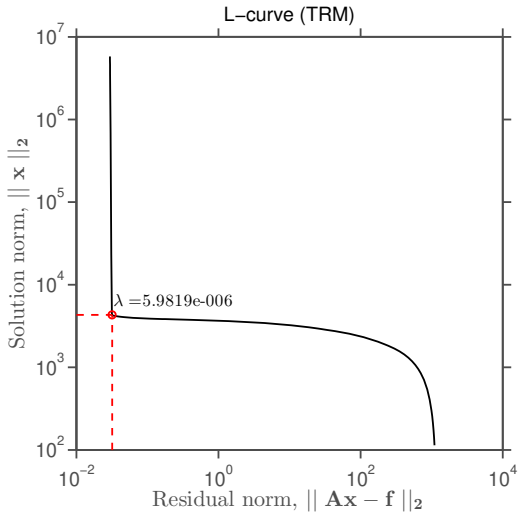

(c) $p_{\boldsymbol{u}} = p_{\boldsymbol{t}} = 5\%$

FIGURE 11. Example 2: The L-curves obtained for various percentages of noise $p_{\boldsymbol{u}} = p_{\boldsymbol{t}} \in \{1, 3, 5\}\%$.

ACKNOWLEDGEMENTS

The authors would like to thank the University of Cyprus for supporting this research. L. Marin acknowledges the financial support received from the Romanian National Authority for Scientific Research (CNCS–UEFISCDI), project number PN–II–ID–PCE–2011–3–0521.

Example 1	1%	3%	5%
$\alpha = 4/3$	2.74×10^{-6}	5.98×10^{-6}	1.04×10^{-5}
$\alpha = 1$	3.42×10^{-6}	7.48×10^{-6}	1.05×10^{-5}
$\alpha = 2/3$	3.42×10^{-6}	8.36×10^{-6}	1.31×10^{-5}
Example 2	1.25×10^{-6}	3.42×10^{-6}	5.98×10^{-6}

TABLE 1. Values of the regularization parameter λ given by the L-curves plotted in Figures 2, 4, 6 and 11 for various percentages of noise $p_{\boldsymbol{u}} = p_{\boldsymbol{t}} \in \{1, 3, 5\}\%$ for Examples 1 and 2.

REFERENCES

[1] G. Alessandrini, L. Rondi, E. Rosset and S. Vessella, *The stability for the Cauchy problem foe elliptic equations*, Inverse Problems **25** (2009), 123004 (47 pp).

[2] M. H. Aliabadi, *The Boundary Element Method. Applications in Solids and Structures*, John Wiley and Sons, London, 2002, Volume 2.

[3] A. Bakushinski, *Remark on choosing a regularization parameter using the quasioptimality and ratio criterion*, U.S.S.R. Comput. Math. Math. Phys. **24** (1984), 181–182.

[4] A. H. Barnett and T. Betcke, *Stability and convergence of the method of fundamental solutions for Helmholtz problems on analytic domains*, J. Comput. Phys. **227** (2008), 7003–7026.

[5] M. Belge, M. Kilmer and E. L. Miller, *Efficient determination of multiple regularization parameters in a generalized L-curve framework*, Inverse Problems **18** (2002), 1161–1183.

[6] C. S. Chen, A. Karageorghis and Y. Li, *On choosing the location of the sources in the MFS*, Numer. Algor., to appear DOI 10.1007/s11075-015-0036-0.

[7] R. Dautray and J.-L. Lions, *Mathematical Analysis and Numerical Methods for Science and Technology, Vol.3, Spectral Theory and Applications*, Springer-Verlag, Berlin, 1990.

[8] B. H. Dennis and G. S. Dulikravich, *Simultaneous determination of temperatures, heat fluxes, deformations and tractions on inaccesible boundaries*, ASME J. Heat Transfer **121** (1999), 537–545.

[9] B. H. Dennis, G. S. Dulikravich and S. Yoshimura, *A finite element formulation for the determination of unknown boundary conditions for three-dimensional steady thermoelastic problems*, ASME J. Heat Transfer **126** (2004), 110–118.

[10] B. H. Dennis, W. Jin, G. S. Dulikravich and J. Jaric, *Application of the finite element method to inverse problems in solid mechanics*, Int. J. Structural Changes in Solids **3** (2011), 11–21.

[11] P. Di Barba and A. Lorenzi, *A magneto-thermo-elastic identification problem with a moving boundary in a micro-device*, Milan J. Math. **81** (2013), 347–383.

[12] G. Fichera, *Existence Theorems in Elasticity*, Springer, Berlin, 1973.

[13] X. W. Gao, *Boundary element analysis in thermoelasticity with and without internal cells*, Int. J. Numer. Meth. Eng. **57** (2003), 975–990.

[14] P. C. Hansen, *Discrete Inverse Problems: Insight and Algorithms*, SIAM, Philadelphia, 2010.

[15] T. I. Ishankulov and O. I. Makhmudov, *The Cauchy problem for a system of thermoelasticity equations in a space*, Mat. Zametki **64** (1998), 212–217.

[16] A. Karageorghis, D. Lesnic, and L. Marin, *The method of fundamental solutions for an inverse boundary value problem in static thermo-elasticity*, Comput. & Structures **135** (2014), 32–39.

[17] A. Karageorghis and Y.-S. Smyrlis, *Matrix decomposition MFS algorithms for elasticity and thermo-elasticity problems in axisymmetric domains*, J. Comput. Appl. Math. **206** (2007), 774–795.

[18] S. Khajehpour and M. R. Hematiyan, *Inverse reconstruction of thermal and mechanical boundary conditions in coupled nonlinear thermo-elastic problems*, Internat. J. Appl. Mech. **6** (2014), 1450014 (33 pages).

[19] V. A. Kozlov, V. G. Maz'ya, and A. V. Fomin, *The inverse problem of coupled thermo-elasticity*, Inverse Problems **10** (1994), 153–160.

[20] J.-L. Lee and Y.-C. Yang, *Inverse problem of coupled thermoelasticity for prediction of heat flux and thermal stresses in an annular cylinder*, Int. Commun. Heat Mass Transfer **28** (2001), 661–670.

[21] L. Marin and A. Karageorghis, *The MFS-MPS for two-dimensional steady-state thermoelasticity problems*, Eng. Anal. Bound. Elem. **37** (2013), 1004–1020.

[22] L. Marin and A. Karageorghis, *The MFS for the Cauchy problem in two-dimensional steady-state linear thermoelasticity*, Int. J. Solids Struct. **50** (2013), 3387–3398.

[23] L. Marin, L., A. Karageorghis and D. Lesnic, *A numerical study of the SVD-MFS solution of inverse boundary value problems in two-dimensional steady-state linear thermoelasticity*, Numer. Methods Partial Differential Equations **31** (2015), 168–201.

[24] L. Marin, A. Karageorghis. and D. Lesnic, *Regularized MFS solution inverse boundary value problems in three-dimensional steady-state linear thermoelasticity*, Int. J. Solids Struct., to appear DOI:10.1016/j.ijsolstr.2016.03.013.
[25] P. L. Mueller and S. Siltanen, *Linear and Nonlinear Inverse Problems with Practical Applications*, SIAM, Philadelphia, 2012.
[26] N. Noda, *An inverse problem of coupled thermal stress in a long circular cylinder*, JSME Int. J. Ser. 1 **32** (1989), 348–354.
[27] N. Noda, F. Ashida and T. Tsuji, *An inverse transient thermoelastic for a transversely-isotropic body*, J. Appl. Mech. **56** (1989), 791–797.
[28] N. Noda, R. B. Hetnarski and Y. Tanigawa, *Thermal Stresses*, Taylor & Francis, New York, 2003.
[29] W. Nowacki, *Thermoelasticity*, second ed., Pergamon Press, Oxford; PWN—Polish Scientific Publishers, Warsaw, 1986.
[30] M. Tanaka, A. Guzik, T. Matsumoto and R. A. Białecki, *An inverse estimation of multi-dimensional load distributions in thermoelasticity problems via dual reciprocity BEM*, Comput. Mech. **37** (2005), 86–95.
[31] Y.-C. Yang, U.C. Chen, and W.-J. Chang, *A inverse problem of coupled thermoelasticity in predicting heat flux and thermal stresses by strain measurement*, J. Ther. Stresses. **25** (2002), 265–281.

Department of Mathematics, Faculty of Mathematics and Computer Science, University of Bucharest, 14 Academiei, 010014 Bucharest, Romania, and Institute of Solid Mechanics, Romanian Academy, 15 Constantin Mille, 010141 Bucharest
E-mail address: marin.liviu@gmail.com; liviu.marin@fmi.unibuc.ro

Department of Mathematics and Statistics, University of Cyprus/ Πανεπιστημιο Κυπρου, P.O.Box 20537, 1678 Nicosia/Λευκωσια, Cyprus/Κυπρος
E-mail address: andreask@ucy.ac.cy

Department of Applied Mathematics, University of Leeds, Leeds LS2 9JT, UK
E-mail address: amt5ld@maths.leeds.ac.uk

EAS, Mathematics, Aston University, Birmingham B4 7ET, UK
E-mail address: johansst@aston.ac.uk